TWO-PART MASTER'S THESIS

PART ONE: EVALUATION OF COOL ROOF REFLECTIVITY IMPACTS

PART TWO: SURFACE SKIMMER FLOW RATES

by

Collin Daine Sharpe

A thesis submitted to the Graduate Faculty of
Auburn University
in partial fulfillment of the
requirements for the Degree of
Master of Science

Auburn, Alabama
May 7, 2022

Keywords: roof reflectance, cool roof, building energy efficiency, solar radiation, surface skimmer, sediment, stormwater, dewatering

Approved by

Michael A. Perez, Chair, Assistant Professor of Civil and Environmental Engineering
Jorge Rueda-Benavides, Co-chair, Assistant Professor of Civil and Environmental Engineering
James S. Davidson, Gottlieb Professor of Civil and Environmental Engineering

PREFACE

This two-part thesis combines two projects of completed while pursuing a Master of Science degree at Auburn University. Part One of this thesis report details the evaluation of cool roof reflectivity and possible detrimental effects of reflectivity. This project was sponsored by the Air Force Civil Engineering Center (AFCEC) through a fellowship with Oak Ridge Institute for Science and Education (ORISE). Part Two of this thesis is based on a study performed at the Auburn University Stormwater Research Facility sponsored by J.W. Faircloth & Son, Inc.

PART ONE: EVALUATION OF COOL ROOF REFLECTIVITY IMPACTS ON NEARBY AIR AND SURFACE TEMPERATURES

ABSTRACT

Cool roofs attempt to lower the temperature of the roof surface so that the interior of buildings can be cooled using less energy. Light color surfaces, white being the coolest color, are much cooler than darker surfaces due to reflectivity. Although several studies have been conducted on the benefits of cool roofs, limited studies have been performed to investigate possible drawbacks of reflective roofing materials on rooftop mechanical and electrical elements, such as heating, ventilation, and air conditioning (HVAC) units. Part One of the thesis presents the research investigating the effects of reflectivity on air and adjacent surface temperatures within 4 ft (1.22 m) above the surface of low-sloped roofs. Although more research is needed on this topic, the existing literature proved that temperature changes a few feet above the roof surface affect the performance of rooftop HVAC units.

Testing was performed at the Auburn University- Stormwater Research Facility in Opelika, Alabama. Two experimental decks were constructed, and each deck was covered with a different roofing membrane. One deck had a white polyvinyl chloride (PVC) membrane, and a black ethylene propylene diene monomer (EPDM) membrane was installed on the other. The experiment was designed to record surface temperatures of the membranes (at the surface level), air temperatures up to 4 ft (1.22 m) above the surface, and temperatures on a nearby surface adjacent to the roof. Testing was conducted from July 2020 until December 2020. An exploratory data analysis was conducted to find initial trends in the data. The final analysis consisted of a comprehensive multiple linear regression (MLR) analysis using data from the top twenty solar radiation values from each testing day. This resulted in various MLR models that use ambient variables such as outdoor temperature, solar radiation, relative pressure, outdoor humidity, and

wind speed to estimate membrane surface temperature and air temperatures from 1 ft (0.30 m) to 4 ft (1.22 m) above the surface for both types of membranes.

The resulting MLR equations were intended to be used by designers to improve cost-effectiveness through decisions associated with the design of roofing structures and the selection of rooftop HVAC units. Higher air temperatures at the inlet of rooftop HVAC units are associated with higher energy consumption. Average local values for the ambient variables on typical warm sunny days can be used in the MLR models to predict surface and over-the-surface temperatures for white and black roof surfaces on buildings in or nearby Opelika, Alabama. Using average ambient values measured at the testing location as independent variables in the final MLR equation, the models predicted air temperature above the white membrane 8.8 ˚F (4.9˚C) higher than ambient outdoor temperature compared to 3.0˚F (1.7˚C) for the black membrane . This resulted in a 10.0% and 3.4% increase from ambient outdoor temperature, respectively. On average, the above surface air temperatures on the white deck were 5.8˚F (3.2 ˚C) higher than the black deck. Additionally, the black EPDM membrane surface reached 130.5˚F (54.7˚C) and the white PVC membrane reached 105.8˚F (41˚C). This corresponds with a 47.8% and 19.8% increase in temperature from ambient outdoor temperature. Adjacent surface temperatures were also significantly higher due to the increased reflectivity of the white PVC membrane.

This is valuable information to building owners and contractors who are aiming to increase building efficiency. These considerations should be accounted for deciding on membrane color, material, and configuration. Climate region and maintenance costs should be considered when selecting a “cool” roofing membrane or coating and not looked at as a universal solution to increasing building energy efficiency.

ACKNOWLEDGEMENTS

The author would first like to thank Dr. Michael A. Perez for his guidance and mentorship throughout the course of this research. The author would also like to thank Dr. Jorge Rueda-Benevides , Dr. Jim S. Davidson, and Dr. Wesley N. Donald for their time, support, and guidance during the research effort. The author would also like to thank the Air Force Civil Engineering Center and Mr. Clayton Deel for the opportunity and financial support throughout the duration of the research; Warren Faircloth, Joe Cooley, and Brian Free for the opportunity and direction provided; and the staff and undergraduate assistants at the Auburn University Stormwater Research Facility for assistance for the entirety of the research. The author would also like to extend gratitude to Logan Duck for countless hours of technical support and advise to aid in the completion of the research. The author would like to especially thank his parents, sister, and brother for their love and unwavering support throughout this process. Finally, the author would like to thank and dedicate this thesis to Steven Kyle Mackey, whose academic achievement and engineering excellence inspired the author throughout his graduate studies.

TABLE OF CONTENTS

LIST OF TABLES

LIST OF FIGURES

CHAPTER ONE: INTRODUCTION

1.1 BACKGROUND

A cool roof is a term referring to a type of roofing system that implements the use of a material and color that reflects light and emits heat, creating a cooling effect on the interior of the building (Testa & Krarti, 2017). Cool roofs have gained significant popularity over recent years and have become implemented in most building codes to help in mitigating urban heat island effects (Gentle et al., 2011; Xu et al., 2012; Yang & Bou-Zeid, 2019). The urban heat island effect is a rise in air temperature in urban cities created by an increase in infrastructure density that absorbs sunlight and emits heat (Heat Island Group, 2022), resulting in increased energy use to cool building interiors. Ibrahim (2009) estimated that 60% of surfaces in urban cities are either roofing or pavement. This high volume of surfaces and heat island effects have increased the use of cool roofs to reflect solar energy, rather than absorb it (Akbari et al., 2009; Li & Norford, 2016; Roman et al., 2016).

Sunlight enters Earth's atmosphere as solar energy and is composed of 5% ultraviolet rays, 43% visible light, and 52% infrared energy (United States Environmental Protection Agency [USEPA], 2008). Infrared light is what is felt as heat on Earth's surface, ultraviolet light is what causes skin to sunburn, and visible light is light that is perceived in the color spectrum (USEPA, 2008). When sunlight encounters a surface on Earth, a portion of the sunlight is absorbed while the rest is reflected into the atmosphere, referred to as albedo (USEPA, 2008). The portion that is absorbed is either transferred through the surface or released into the atmosphere as heat by conduction, radiation, and convection (Dupuis, 2014). When heat is absorbed, the roof will begin a process of releasing absorbed heat until it reaches a state of equilibrium with ambient conditions,

a well-known law of thermodynamics. Cool roofs are characterized and rated based on the material's albedo. Cool roofs that are white in color have a higher albedo than a roof that is black in color. For example, a highly reflective roof can have an initial reflectance up to 85-90%, while a dark colored, non-reflective, roof will only reflect 5-15% of the incoming sunlight (USEPA, 2008).

A low-sloped roof refers to a surface that has a slope of 2V:12H (16.7%) or less, corresponding to a 9.5° angle (ASTM E1918). Various classifications of buildings have roofs that are low sloped, such as commercial and industrial buildings in urban and rural areas. The most common materials used on low-sloped roofs are thermoplastic polyolefin (TPO), PVC, EPDM, and traditional asphalt coatings (Ibrahim, 2009). TPO, PVC, and EPDM are classified as single-ply membranes, which are prefabricated sheets that are applied to a low-sloped roof by using an adhesive or mechanical fastener and are either heat welded or glued at the seams (USEPA, 2008). Although there are numerous manufacturers for single-ply membranes, they are all categorized by the same values. Common values found representing membranes are solar reflectance, thermal emittance, and solar reflectance index (SRI). Several testing standards have been developed to measure these parameters.

Solar reflectance is the percentage of incoming sunlight, or radiation, which is reflected off the membrane. ASTM E1918 is a common standard used to measure solar reflectance. Thermal emittance is a ratio of radiative energy released (ASTM C1371). The SRI value combines solar reflectance and thermal emittance into one representative value. The value is ranked from 0 to 100 with zero considered as a standard black material and 100 a white material (ASTM E1980). Thus, the closer the SRI value is to 100, the "cooler" the material is considered. The Cool Roof Rating Council (CRRC), Leadership in Energy and Environmental Design (LEED™), and ENERGY

STAR set standards for the values described above of what constitutes as a cool roof. For example, a low-sloped roofing material must have an initial SRI value of 82 and a 3-year aged SRI of 64 to be LEED certified (CRRC, 2022).

There has been extensive research performed on the benefits of cool roofs (Jo et al., 2010; Levinson & Akbari, 2010) indicating energy savings up to 20%-40%. These studies are based on software that model building efficiency without accounting for above surface environment on the roof and its effect on rooftop equipment such as HVAC systems and PV panels. Although cool roofs have significant benefits, current models may be underestimating the extent of potential savings and efficiency, which may be increased due to effects reflective roofing materials have on nearby air and surface temperatures.

1.2 RESEARCH OBJECTIVES

The main objective of this study was to investigate temperature profiles generated up to four feet over reflective roof surfaces under the premise that potential higher temperatures above the surface and adjacent walls could affect the performance of rooftop equipment, such as HVAC units. The study has developed recommendations that will minimize effects of reflected solar radiation on rooftop equipment. That objective was achieved through the recording of air and surface temperatures at various heights above roofing materials with various reflectivity. The study was designed so that a comparison between materials could be made easily. This research was divided into three primary components:

(1) Conduct a comprehensive literature review of cool roof materials, reported energy savings, and similar studies evaluating effects of cool roof reflectivity

- Compile findings from literature review and catalog similar studies to determine possible test strategies.

(2) Design, construct, and evaluate experimental tests to determine how reflectivity influences surface and air temperatures up to 4 ft (1.22 m) above the roof surface.

- Compile findings from literature review and catalog similar studies to determine possible test strategies.
- Construct experimental decks and apply roofing membrane materials with different reflectivity.
- Assemble a data collection strategy and develop a procedure for recording air and surface temperatures at various heights up to 4 ft (1.22 m) above the roof surface.
- Process and analyze data to investigate trends and develop a predictive model for temperature fields above experimental roofs.

(3) Develop a final report detailing the findings and suggest recommendations for improvement.

- Present results of experimental tests, provide guidance for mitigating detrimental effects of reflectivity, propose implementable strategies, and suggest possibilities for furthering the research.

1.3 EXPECTED OUTCOMES

The expected outcome of this research is to provide the cool roof industry with knowledge to improve effectiveness of cool roofing materials and not assume a cool roof is a universal solution to improving building energy efficiency. This research will provide an understanding of the importance of considering the environment above the rooftop and to consider the entire roofing assembly. This study will also explain the need for considering local climate conditions when selecting the roofing material. Moreover, further research efforts should emanate from this study, yielding future opportunities to extend knowledge of cool roof materials and color selection for low-sloped roofs.

1.4 ORGANIZATION OF PART ONE

Part One of the thesis is divided into six chapters that encompass the approach taken to meeting the defined research objectives. Following this chapter, Chapter Two: *Literature Review*, provides an overview of cool roof benefits and catalog previous studies similar to this research. Chapter Three: *Means and Methods*, details experimental design, testing regime, data collection, and an exploratory data analysis approach to investigate effects of reflectivity. Chapter Four: *Analysis of Results*, explains the process of creating multiple linear regression models and determining the highest performing model. Chapter Five: *Discussion and Recommendations*, examines the findings from the exploratory data analysis and the results, as well as provides recommendations for improvements and possible solutions. Chapter Six: *Conclusion*, provides a comprehensive summary of the research and gives insight to further research opportunities.

CHAPTER TWO: COOL ROOF LITERATURE REVIEW

2.1 DEFINITION AND PURPOSE OF COOL ROOFS

Cool roofs are reflective roofing materials classified by high solar reflectance and thermal emittance. Cool roofs are typically white in color and applied by either a single ply membrane or liquid coating. High reflectance and emittance reduce the amount of heat absorbed by the roof which decreases heat flux through the roofing assembly and into the building. Decreasing flux to the interior of the building can reduce the energy loads on HVAC equipment to cool the building in warm to hot weather conditions. Cool roofs are designed to increase energy and financial savings for building owners. The effectiveness and potential benefits of cool roofs have been well researched and are commonly estimated using building performance simulations (BPS) (Hopfe & Hensen, 2011; Jo et al., 2010; Mastrapostoli et al., 2014; Romeo & Zinzi, 2013; Seifhashem et al., 2018; Synnefa et al., 2012). BPS practices use local ambient weather conditions to estimate air temperature at an HVAC intake and do not account for changes in the temperature gradient above the roof caused by roof material and color.

2.2 BUILDING PERFORMANCE SIMULATION PRACTICES

Building performance simulations are used to form mathematical models which predict building energy consumption based on physical properties. Architects and engineers commonly use BPS practices to evaluate energy consumption and overall cost efficiency of buildings. In a study conducted by Levinson and Akbari (2010) BPS practices, local energy prices, local electricity emission factors, and local estimates of building density were combined to characterize local, state, and national average cooling energy savings, heating energy penalties, energy cost savings, and emission reductions per unit conditioned area of roof. This study reported that by

retrofitting 80% of the 27.8 billion ft^2 (2.58 billion m^2) of commercial building conditioned roof area in the United States with reflective roof coatings (solar reflectance 0.55) would generate an annual cooling energy saving of 10.4 TWh, and an annual heating energy penalty of 3.9 TWh. This resulted in an annual cost reduction of $735 million. It has been estimated that a 1% to 2% reduction in temperature at HVAC fresh air intakes can result in a reduction in energy consumption by 1.44%, on average (Green et al., 2020). Based on this finding, the cost savings reported by Levinson and Akbari could be off by $10-$20 million. This is because BPS practices neglect the influence of roof surface temperature and reflectivity on above-roof air and nearby surface temperatures.

2.3 EXPERIMENTAL EVALUATIONS OF ROOF REFLECTIVITY

When comparing surface temperatures of a conventional black roof to a white cool roof, the surface temperature of the black roof has been proven significantly warmer than the cool roof. Ibrahim (2013-2) took temperature measurements of a black EPDM membrane and a white TPO membrane during July and August of 2011. Temperatures were recorded at the roof surface and at heights of 10, 16, 22, and 34 in. (25.4, 40.6, 56, and 86.4 cm) above the two membranes. The research reported surface temperatures of the black EPDM membrane ranging from 11 to 47.3 °F (6.1 to 26.3 °C) above ambient air temperature while the white TPO membrane ranged from 17 to 23 °F (9.4 to 12.8 °C) above ambient air temperature. Although surface temperatures were significantly higher for the black EPDM membrane, air temperatures above the surface were consistently higher above the white TPO membrane at each height. Ibrahim states that these temperature increases could result in energy losses between 14% and 18%.

Grant et al. (2017) conducted a similar study considering air temperatures at various heights above a low-sloped roof in 2016 while ambient air temperature was at 26 °C (78.8°F).

They incorporated temperature effects of the roofing membrane on an adjacent precast concrete wall. This study also compared a black EPDM membrane and a white TPO membrane. Their findings on air temperatures at heights of 8, 14, 23, 86 cm (3.1, 5.5, 9.1, and 34 in.) and above the roof surface did not show that the white TPO membrane produced higher temperatures at all heights except at 86 cm (34 in.). At this height, air temperature was slightly higher above the TPO membrane than the black EPDM membrane. This finding is important because this is close to the height at which most HVAC intakes are located. The lower heights at which air temperature was recorded are not even one foot above the surface. At that height, surface temperatures and heat emitting from the membranes are likely affecting air temperatures, rather than reflectivity. For the adjacent precast concrete wall, temperatures were recorded at heights of 56, 86, 132, and 162 cm (22, 34, 52, and 63.8 in.) above the roof surface. Each of the four height intervals recorded higher surface temperature averages above the white TPO membrane than the black EDPM membrane. At 56 cm (22 in.) the least squares mean difference in the two was 3.4°C, 2.96 °C at 86 cm, 5.14 °C at 132 cm, and 5.24 °C at 162 cm (6.07°F, 5.33 °F at 34 in., 9.25 °F at 52 in., and 9.43 °F at 63.8 in.). Temperatures of the precast concrete wall were recorded at higher distances above the roof surface than air temperature recordings. At an increased height, temperature increased is influenced strictly by reflectivity and not emittance of surface heat.

In a previous study conducted by Green et al. (2020), field experiments were conducted to evaluate the effects of reflectivity on the air temperature field above low-sloped roofs of three shopping center buildings near Sydney, Australia. Tests were conducted during summer and spring seasons and the roofs were monitored over a span of six weeks. Roofing materials on each building were not uniform and varied in reflectivity across the roof. Solar reflectance was measured according to ASTM E1918 standards and thermal emittance measured by ASTM C1371 standards.

The three buildings' roofs were labeled as Roof A, Roof B, and Roof C. Roof A had a total roof area of 15,978 m^2 (171,986 ft^2) and was composed mostly of aged bare metal-coated steel with solar reflectance of 0.27 and thermal emittance 0.63. Roofs B and C were much larger than Roof A and were composed of metal-coated steel, concrete, and steel with a field applied cool coating. The steel with a field-applied cool coating had a solar reflectance of 0.61 and thermal emittance of 0.85. Air temperature above each roof was measured from 0.5 to 1.5 m (1.64 to 4.92 ft) above the surface. Ambient temperature was measured at 8 m (26.25 ft) above the buildings' roof surfaces. On average, air temperatures recorded 0.5 to 1.5 m (1.64 to 4.92 ft) above the roof surface reached 2.96˚C, 2.73˚C, and 1.89˚C (5.33˚F, 4.91˚F, and 3.40˚F) above ambient temperature during the day and 1.58˚C, 1.14˚C, and 1.27˚C (2.84˚F, 2.05˚F, and 2.29˚F) below ambient temperature at night for buildings A, B, and C, respectively. In some instances, air temperature above the roofs reached 5˚C (9˚F) above ambient air temperature. These findings are significant, but experimental testing was performed on primarily "non-cool" roofs. This study did not conduct experiments on cool roofing membranes to compare findings.

These results are significant because over time, increased temperatures on adjacent surfaces and roofing materials will accelerate the aging process, resulting in higher maintenance or replacement costs. Also, temperature increases above ambient would lead to incorrect energy savings reported by conventional building simulation practices. These studies show that there is a correlation between membrane color and air temperatures above the membrane. The studies' results proved the white TPO membrane increased either air temperature above the roof or surface temperature of an adjacent wall, a result of higher albedo of the white membrane. A white surface will reflect solar radiation away from the surface which will decrease the surface temperature of the roof but will increase the air temperature above the roof. Although studies have shown potential

energy savings of 2% to over 40%, and averaged about 20% (Pisello et al., 2013), these estimations are likely derived from simulations that do not consider the rooftop environment as a whole. In this study, the conditions above the rooftop will be studied closely so possible solutions can be recommended to improve building efficiency.

CHAPTER THREE: MEANS AND METHODS

3.1 INTRODUCTION

This section describes the experimental design and testing regime developed for the controlled small-scale testing of cool roof materials to study the effects of reflectivity. The methodology developed for the experimental design and data collection procedures are derived from examination of previous studies. This methodology best aims to provide evaluations of high-reflectance cool roofing materials and traditional low-reflectance roofing materials. The testing procedures and evaluations are subjected to ambient weather conditions typically found in the Southeast, specifically Alabama.

The purpose of the experiment is to investigate the effect of reflectivity up to 4 ft (1.22 m) above a white membrane and provide recommendations to mitigate unintended effects. The experiments are conducted on a white PVC membrane and a black EPDM membrane to make a comparison between highly reflective and extremely low reflective materials. Performance of each roofing material is compared to ambient conditions to develop a predictive model through an exploratory data analysis process.

3.2 DECK CONSTRUCTION

The Auburn University-Stormwater Research Facility on the South hill served as the test site. This site was selected due to its accessibility, and it provided a clear and open area where trees or other structures would not block any sunlight from the experiment. Testing was conducted on two decks that were assembled with wooden boards and plywood. Both decks were designed as 8 ft by 8 ft (2.44 m by 2.44 m) and were 2 ft (0.61 ft) above the ground. A vertical plywood wall was attached on one side of each deck and stood 4 ft (1.22 m) tall from the platform. The

walls were attached to evaluate different ways reflectivity affected adjacent surfaces. The decks were positioned with walls facing directly South. This was the position that exposed the deck surface and walls to the most sunlight intensity. Finally, a black EPDM membrane and a white PVC membrane were applied to the deck using a PVC adhesive. The decks are shown in Figure 1 (a) and (b).

(a) White membrane deck **(b) Black membrane deck**

Figure 1 Experimental Decks.

The white membrane used for testing consisted of a PVC material from IB Roofing Systems™. The membrane was type three (internally reinforced with fabric) and met ASTM D4434-12 standards. The PVC membrane had a solar reflectance value of 0.87, a thermal emittance of 0.88, and an initial SRI value of 110. The membrane was fully adhered to the wooden deck using the IB Roofing System's VertiBond® Adhesive. Specifications were not provided on the EPDM membrane, but generally a black EPDM membrane has a solar reflectance less than 0.05 and a thermal emittance close to that of the PVC (0.80-0.90).

3.3 TESTING EQUIPMENT AND CONFIGURATION

Air temperature above each deck was recorded at 1, 2, 3, and 4 ft (0.31, 0.61, 0.91, and 1.22 m) above the surface. A PVC pipe stand was constructed using a 5 ft (1.52 m) tall vertical base pipe with a 1-in. (2.54 cm) diameter and four staggered pipes with a 0.5-in. (1.27 cm) diameter at 1, 2, 3, and 4 ft (0.31, 0.61, 0.91, and 1.22 m) above the deck surface. This prevented any of the horizontal arms from blocking or affecting any reflected sunlight or heat emitted from the surface to the arm directly above it. Each PVC stand was configured with four temperature probes to record air temperature, one surface temperature sensor probe, and two wall surface temperature sensors, as illustrated in Figure 2, showing the experimental model design.

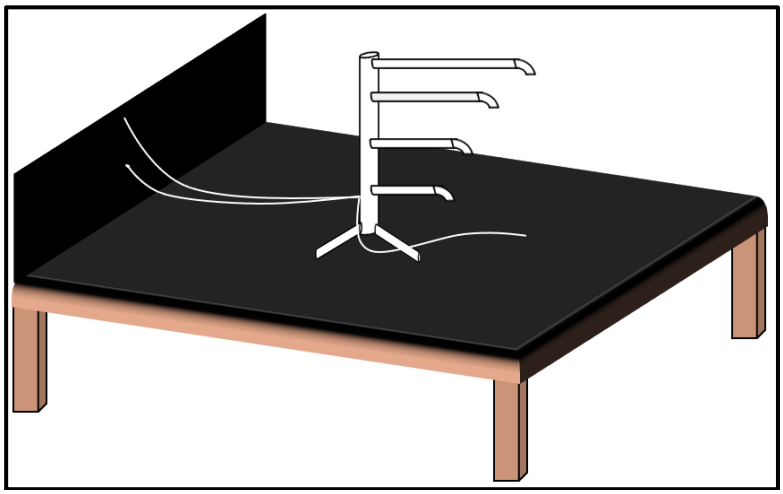

Figure 2 Modeled Setup for Temperature Testing.

All sensors were DS18B20 model, capable of recording temperatures ranging from -67°F to 257 °F (-55 to 125 °C) and have an accuracy of ±0.5 °F (0.28 °C). Surface and adjacent wall temperature sensors on the black EPDM deck were secured with black electrical tape and the white PVC deck with white electrical tape to mimic SRI values of each roofing material. Sensors recorded temperatures simultaneously on each deck along with temperature recordings from a

nearby Ambient Weather WS-2902C weather station on the South hill. Table 1 lists the equipment used for each deck.

Table 1 Testing Equipment for Temperature Recordings

Equipment	Description	Quantity
DS18B20	Stainless steel temperature sensor probe	14
CanaKit Raspberry Pi 3 B+	Data loggers attached to temperature sensors	2
MD-D1144-1	Pi screw terminal block breakout module	2
Ambient Weather® WS-2902C	WiFi smart weather station	1

Each of the sensors were lengthened appropriately and fed up the vertical PVC pipe and down the arm to the end. The wiring for the sensors were attached to the module on top of the Raspberry Pi 3 B+. The Raspberry Pi 3 B+ was then programmed to collect and store the data and encased in a weatherproof electrical box. Figure 3(a) is the Raspberry Pi 3 B+, Pi screw terminal block breakout module, and DS18B20 sensors once fully assembled with the wiring configuration. Figure 3(b) is an image of the Ambient Weather WS-2902C weather station. All fourteen temperature sensors on both decks simultaneously recorded temperature every five minutes for 24 hours a day.

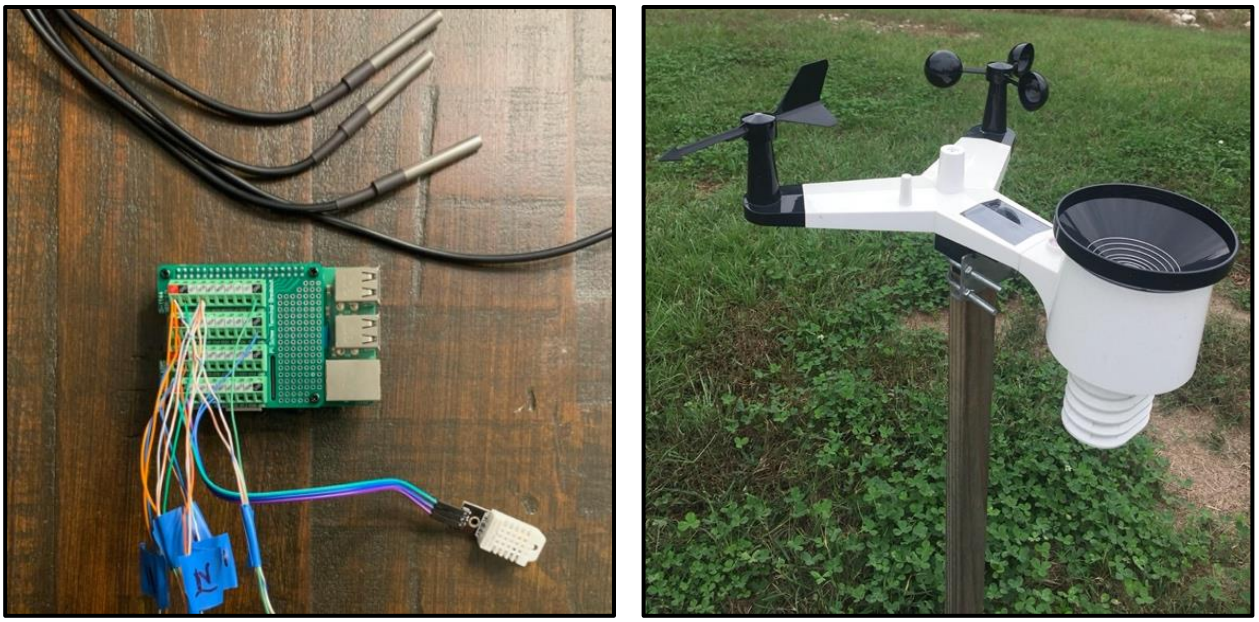

(a) Assembled data collection equipment **(b) Ambient Weather WS2902-C**

Figure 3 Equipment for Data Collection.

3.4 DATA COLLECTION AND MANAGEMENT

3.4.1 Methods

Data was collected daily from the months of July 2020 to December 2020. Temperature was recorded in five-min intervals for 24 hours to get a complete understanding of how air temperatures above each surface changed with ambient conditions. To start, surface temperatures of the walls were taken directly on the membranes themselves. After realizing that surface temperatures recorded on adjacent walls were being affected by the membranes themselves, a 2 ft wide 4 ft tall (0.61 m wide 1.22 m tall) plywood board was vertically mounted over the membranes in the center of each wall to better study the effects of reflectivity. Although plywood is not a representative material or commonly found on a low sloped rooftop, a relative comparison could be made between the two decks. Surface temperature sensors for the walls were mounted with

electrical tape matching SRI of roofing material at 2 ft and 4 ft (0.61 m and 1.22 m) above the surface of each deck. Figure 4(a) displays the 4 ft tall plywood board mounted on the wall of each deck. Figure 4(b) shows how each PVC arm on the stand had a 90° downward facing extension, in lieu of traditional radiation shields, to partially shield temperature sensors from direct solar radiation. This allowed the effects of reflectivity on air temperature to be studied without the influence of direct radiation from incoming sunlight. Figure 4(c) shows both decks with stands in place.

(a) Mounted Plywood on adjacent wall

(b) PVC arm extension with temperature sensor

(c) Experimental setup with stands in place

Figure 4 Experimental Decks with Testing Equipment.

3.4.2 Data Collection and Management

3.4.2.1 Raspberry Pi and Sensors

The Raspberry Pi 3 B+ (Pi) code was written to collect temperature readings from the sensors in 5-minute intervals, 24 hours a day. The two Pi's were synchronized, thus recorded temperatures at the same time. Sensors were labeled both within the coding and on the sensor itself to ensure each sensor was in its correct position. A module installed on top of each Pi allowed for each sensor to be connected. The Pi's were connected to the Wi-Fi at the AU-SRF and were capable of remote login. Having the capability of remote login allowed the ability to download data, obtain updates on activity, and identify and troubleshoot any issues instantly. This was important because data collection was continuous, and the Pi's could be checked daily to ensure all systems were functioning properly. Temperature recordings were stored in multiple files within each Pi and stored in a microSD card to ensure the safety of all data collected. Data could be downloaded from the Pi via remote login. The dates and times of the data needed could be selected and downloaded on to a personal laptop as a comma-separated values (CSV) file. The CSV file could then be converted into Microsoft Excel format to begin to form the database. Raw data included date, time, and temperature recordings for 14 sensors. Sensors recorded temperature to the thousandths. Figure 5 is an example of raw data from the Pi once converted to Microsoft Excel format.

			Black							White						
id	date	time	temp_0	temp_1	temp_2	temp_3	temp_4	temp_5	temp_6	temp_0	temp_1	temp_2	temp_3	temp_4	temp_5	temp_6
1	7/21/2020	9:48	130.887	94.212	89.15	91.512	91.85	108.837	103.1	103.1	98.487	97.137	97.25	96.35	104	98.712
2	7/21/2020	9:53	131.45	92.975	89.262	92.187	92.525	110.3	105.575	104.675	101.412	99.837	98.937	97.925	105.8	101.862
3	7/21/2020	9:58	135.275	96.462	91.962	95.9	96.125	113.225	109.625	107.262	102.65	103.1	102.537	102.425	108.387	104.9
4	7/21/2020	10:04	137.075	94.887	92.412	95.112	95.225	114.125	111.087	108.05	102.762	103.55	102.425	101.525	108.725	105.8
5	7/21/2020	10:09	132.462	94.887	92.075	93.312	93.537	111.875	108.725	105.462	99.612	100.625	100.287	100.287	105.912	102.65
6	7/21/2020	10:14	129.875	93.65	91.062	92.3	92.3	110.187	106.7	104.112	96.012	95.45	95.562	95.112	103.325	98.825
7	7/21/2020	10:19	131.562	95	91.85	92.975	93.312	111.425	107.6	105.8	97.137	96.125	95.9	95.225	105.575	99.95
8	7/21/2020	10:24	136.85	92.525	91.85	92.975	93.312	115.7	109.962	108.95	98.937	98.037	98.15	97.137	110.3	102.2
9	7/21/2020	10:29	139.662	92.187	91.512	92.637	92.975	117.275	110.412	109.625	98.825	98.937	100.175	99.275	111.087	103.437
10	7/21/2020	10:34	140.225	95.112	93.987	95.112	95.225	117.837	113.112	111.2	102.2	101.862	101.75	101.75	112.662	106.587
11	7/21/2020	10:39	142.025	93.762	93.312	94.212	94.55	118.962	113	111.2	102.537	102.312	102.312	101.525	113	106.475
12	7/21/2020	10:44	140.675	93.312	92.187	93.312	93.537	117.05	109.512	108.275	98.15	97.7	99.275	98.375	110.862	101.187
13	7/21/2020	10:50	140.112	95.45	93.425	94.212	94.437	116.487	110.75	109.062	100.625	100.062	100.85	99.837	111.762	104.112
14	7/21/2020	10:55	143.712	96.125	94.437	95	95.225	119.75	110.75	112.212	104	103.662	103.55	102.875	114.35	107.825
15	7/21/2020	11:00	144.612	96.462	95.337	95.675	95.675	119.862	113.675	113.337	105.012	104.45	104.45	103.1	115.025	107.6
16	7/21/2020	11:05	145.287	98.375	96.8	96.912	96.8	120.537	115.362	113.9	105.912	105.35	105.012	104.112	116.15	109.062
17	7/21/2020	11:10	146.975	99.725	97.362	97.25	97.475	121.55	116.037	114.8	106.7	106.475	105.687	104.562	115.925	110.075
18	7/21/2020	11:15	147.987	97.362	95.45	95.675	95.787	121.437	114.687	111.537	102.537	103.325	105.462	104.787	114.912	105.8
19	7/21/2020	11:20	146.637	97.475	94.775	95.45	95.9	120.762	113.562	113.337	102.537	102.087	102.875	101.637	115.025	106.362
20	7/21/2020	11:25	149.225	100.062	96.575	97.025	97.475	123.237	116.6	113.225	101.525	100.625	101.975	100.512	115.925	105.462
21	7/21/2020	11:30	145.737	97.137	94.325	94.887	95.337	120.875	113.675	112.662	102.762	101.525	101.412	100.175	113.225	106.137
22	7/21/2020	11:35	143.262	97.587	95.112	95	94.887	119.3	114.35	111.875	103.775	102.312	100.85	100.287	111.762	106.25

Figure 5 Raspberry Pi 3 B+ Raw Data Output.

3.4.2.2 Weather Station

An Ambient Weather ® WS-2902C weather station was used to record ambient conditions. Conditions such as outdoor temperature (˚F), solar radiation (Watts/m^2), outdoor humidity (%), relative pressure (inHg), and wind speed (mph) were recorded and stored in an online website used to access the weather station. Through the Ambient Weather® website, current ambient conditions could be accessed as well as conditions from past testing dates. Daily data on the conditions listed above could be viewed in graphs and data could be downloaded into a CSV file for any specified date range. The CSV file could then be converted to Microsoft Excel format and merged with temperature recordings from the Pi's. Time of recording from the weather station were closely matched with recording time of the Pi's. Like the Pi's, the weather station collected and recorded ambient weather conditions in 5-minute intervals daily. It was important that the weather station was synchronized with the Pi's so that it could be observed how sudden changes in ambient conditions affected temperature recordings on the decks. This way correlations between data from deck sensors and ambient variables from the weather station could be made. The weather station was placed on the same hill as the two experimental decks and was approximately 5 ft (1.52 m)

above the ground. Sensors used to record temperatures above experimental decks were placed above natural ground next to the weather station to ensure readings between the two were similar. Temperature recordings from the sensors were within 1 to 2˚F (0.55 to 1.11˚C), at most, with the weather station. Therefore, no calibration of the sensors or adjustment of data was needed to compensate.

3.5 EXPLORATORY DATA ANALYSIS

3.5.1 Preliminary Analysis

To begin the data analysis process, daily temperature recordings from deck sensors and ambient conditions from the weather station were combined in Excel and plotted against time to find initial trends in the data. Temperature recordings for each sensor on the white deck were plotted with the corresponding sensor from the black deck, along with outdoor temperature recorded by the weather station. Example graphs are provided in Figure 6 from August 12, 2020. Daily highs for ambient conditions are as follows: outdoor temperature (94˚F) (34.4˚C), solar radiation (938 Watt/m^2), outdoor humidity (66%), relative pressure (29.86 inHg) (101.1 kPa), and wind speed (5.4 mph) (2.41 m/s). Figure 6(a) shows temperature from each deck surface and ambient temperature. As expected, surface temperatures on the black EPDM deck are much higher than temperatures on the surface of the white PVC deck. This is due to the white material reflecting sunlight while the black material absorbs sunlight, heating the surface. This is the reasoning behind cool roofs and lowering surface temperature and heat transfer from the roof and into the building.

Figure 6(b) displays sensors placed 4 ft (1.22 m) above the surface of the white and black decks, along with ambient temperature. This figure shows that temperatures at 4 ft (1.22 m) above the white deck are higher than corresponding temperatures above the black deck during the warmest part of the day. This was an important finding in the study because it validated the

question of whether reflectivity would affect temperatures up to 4 feet above the roof surface. Graphs for sensors at 1, 2, and 3 ft (0.31, 0.61, and 0.91 m) above the white deck were like the 4 ft (1.22 m) sensor graph and were higher than temperatures above the black deck. Figure 6(c) shows temperature recordings 2 ft (0.61 m) high on the mounted plywood walls for each deck. These temperature recordings, as well, were higher on the white deck than the black deck, giving further evidence of reflectivity affecting nearby surface temperatures.

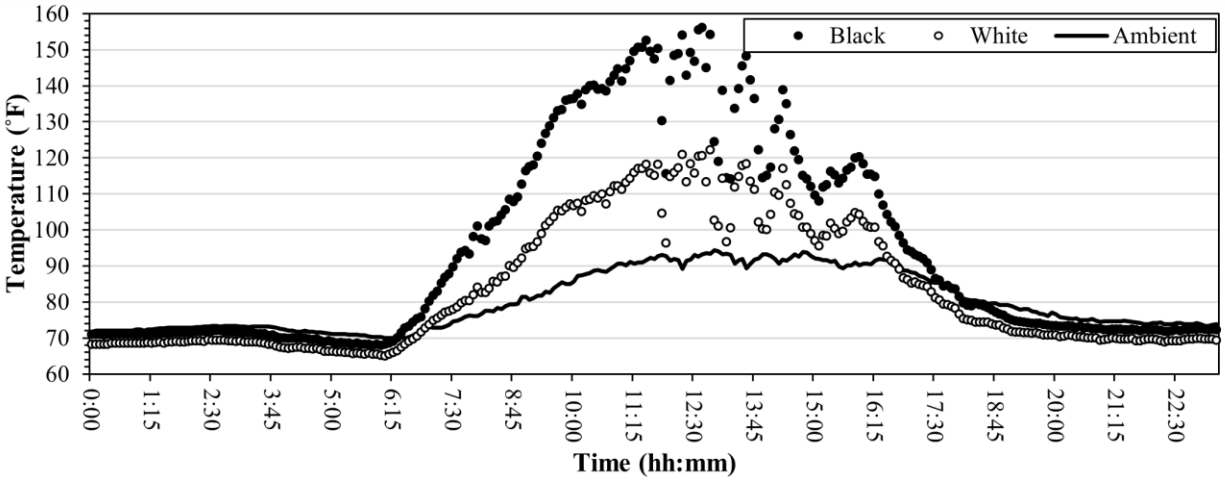

(a) Surface Temperature vs. Time

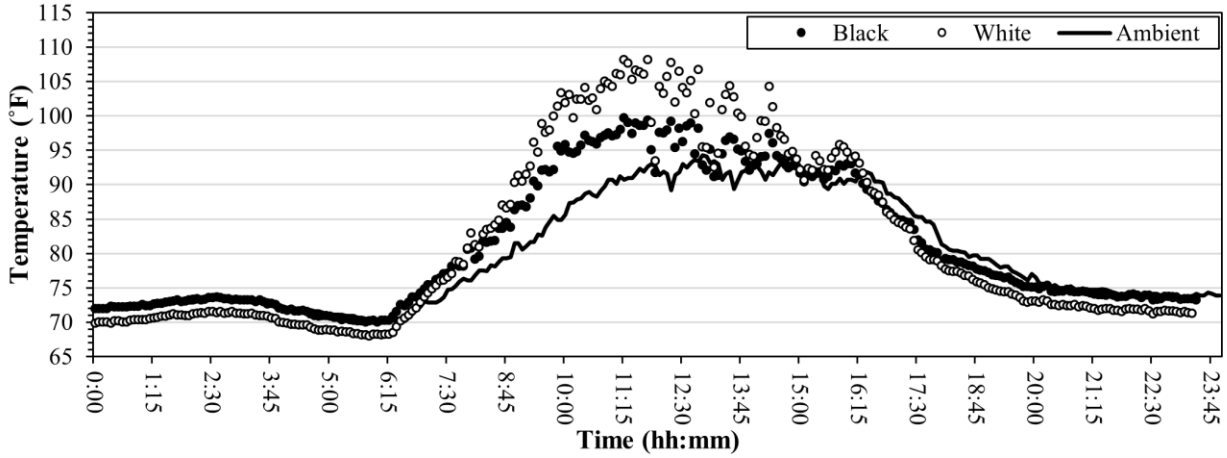

(b) 4-ft Air Temperature vs. Time

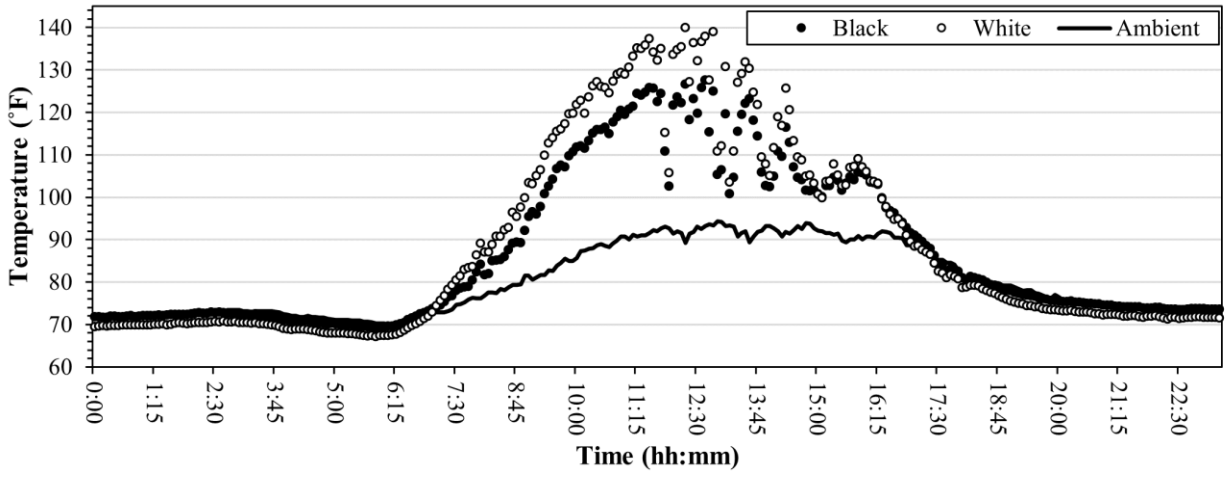

(c) Wall 2-ft Surface Temperature vs. Time

Figure 6 Graphs from Preliminary Analysis (08/12/2020).

Upon further investigation, it was discovered that temperature recordings on the adjacent wall had a high degree of variability. This is likely due to temperature sensors being mounted on the plywood wall which likely resulted in inconsistencies in temperature recordings over the span of testing. As a result, temperature recordings on the adjacent wall were not used in further analyses. It is still important to note that reflectivity of the white membrane increased temperature recordings when compared to the black membrane and ambient outdoor temperature.

This analysis method was performed for several sunny days in the months of July, August, and September. Though ambient conditions varied, the results found on other days analyzed were like those found on August 12, 2020. This preliminary analysis was important in finding trends in the data and making observations. Although this process provided useful information and visuals, there needed to be a way of combining daily data to better summarize trends and create a model.

Next, the process of creating a model to predict temperatures up to 4 ft (1.22 m) above the deck surfaces was initiated by determining the model parameters. The research was to be conducted on warm to hot days in summer and fall months. Clouds blocking sunlight result in lower solar radiation values but do not necessarily result in lower ambient temperatures. To properly study the effects of roof reflectivity, the database was constructed using the top 20 solar radiation values for each day of testing.

Solar radiation was chosen as the reference variable to select critical observations each day because peak values in solar radiation best align with peak values in the temperature sensors on each deck. Figure 7 below displays the temperature recordings on each deck for the sensor located 4 ft above the deck (Figure 7(a)) and at the surface of the deck (Figure 7(b)). Solar radiation was plotted on the secondary axis to illustrate how the peak values of solar radiation better aligned with sensor temperature than ambient outdoor temperature. On sunny days, there were approximately

20 solar radiation recordings during the time frame of peak values. Extracting the daily top 20 solar radiation values was the best method of evaluating reflectivity and provided a large enough dataset to create the model. Multiple linear regression (MLR) was identified as the most effective data analysis method to create the model. Independent variables for the MLR models were ambient conditions recorded by the weather station and dependent variables included all sensors on the white and black decks. Independent were determined by the practicality of a user having the weather conditions readily available and the reliability and significance of the data recorded by the weather station.

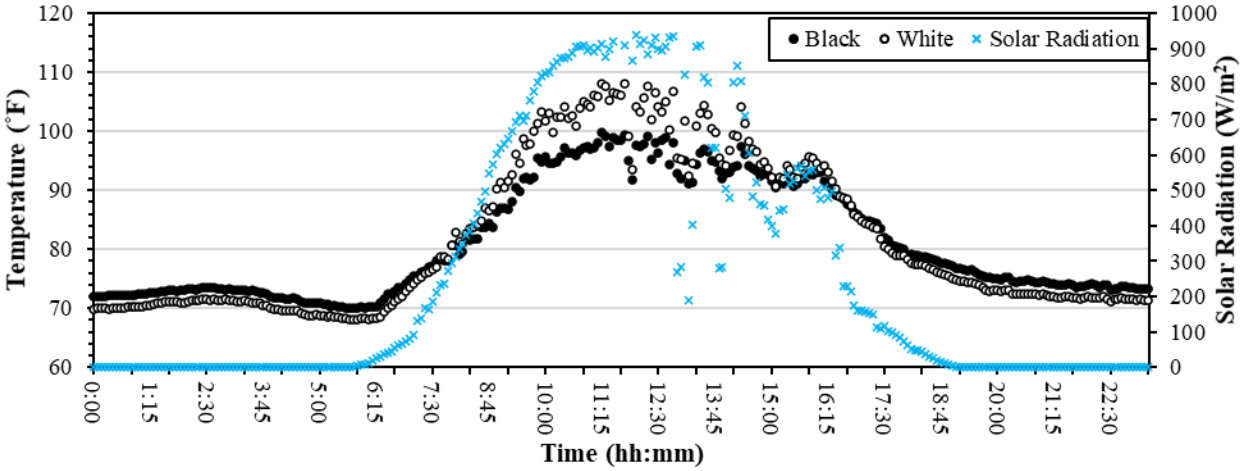

(a) 4-ft Air Temperature vs. Time

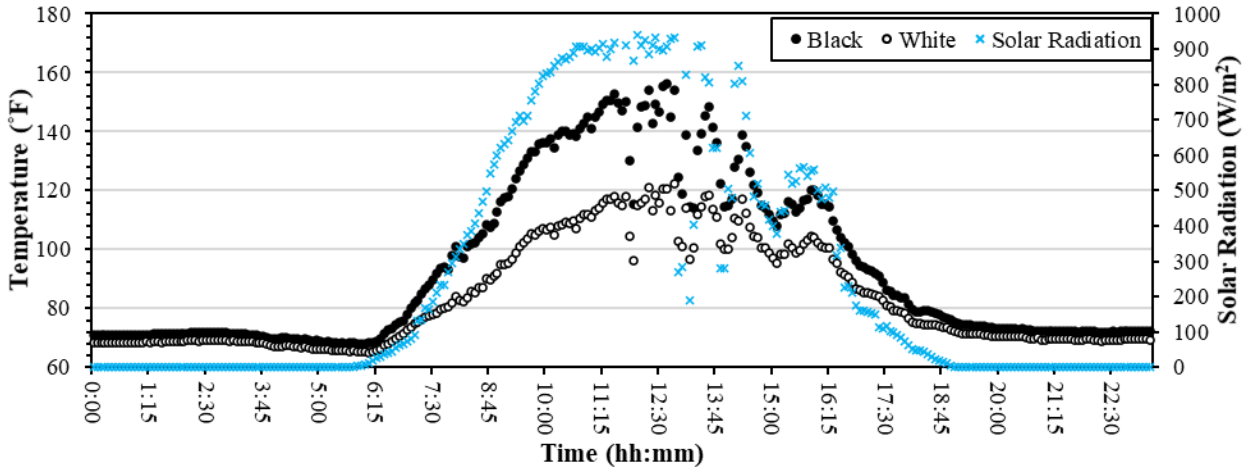

(b) Surface Temperature vs. Time

Figure 7 Deck Sensor Temperature and Solar Radiation (08/12/2020).

3.6 DATA PROCESSING AND MULTIPLE LINEAR REGRESSION ANALYSIS

3.6.1 Defining variables

The first step in data processing was to combine temperature recordings from the sensors with data from the weather station. Since both the sensors and weather station recorded data in 5-min intervals, the dates and times could be matched when combining. This was necessary to observe how temperature recordings from the sensors changed along with ambient conditions during a testing day. The date range for raw data used to create the database ranged from July 14, 2020, until December 16, 2020.

Next, the top 20 solar radiation values were identified for each day of testing and corresponding data was extracted for the observation. In this study, an observation was defined as a set of values recorded at a specific time by temperature sensors on the decks and the weather station. Table 2 below includes the identification (ID) and description of each variable used in the study.

Table 2 Variables for Data Analysis

	ID	Description
Ambient Variables	X1	Outdoor Temperature (˚F)
	X2	Solar Radiation (Watt/m^2)
	X3	Outdoor Humidity (%)
	X4	Relative Pressure (inHg)
	X5	Wind Speed (mph)
Sensor Variables	Black_0	Black Surface Temperature
	Black_1	Temperature 1 Foot Above Black Surface
	Black_2	Temperature 2 Foot Above Black Surface
	Black_3	Temperature 3 Foot Above Black Surface
	Black_4	Temperature 4 Foot Above Black Surface
	White_0	White Surface Temperature
	White_1	Temperature 1 Foot Above White Surface
	White_2	Temperature 2 Foot Above White Surface
	White_3	Temperature 3 Foot Above White Surface
	White_4	Temperature 4 Foot Above White Surface

3.6.2 Outlier Detection and Removal

Outlier detection was necessary for this study to remove outlying values caused by any unexpected factors in instrumentation or improperly recorded data. Outliers in a dataset used to create data-driven models have the potential to influence the performance of the model (Pakalapati, 2018). The Modified Z-Score Method was chosen as the method of detecting and removing outliers in the dataset. The Z-score method used the mean and standard deviation to detect outliers in a normally distributed dataset. Outliers can sometimes go undetected, and z-scores can be affected by extreme values (Seo, 2006). The modified Z-score method uses the median of the values and the absolute deviation of the median. Therefore, the modified z-score method was more appropriate for detecting outliers in solar radiation values. Solar radiation values recorded by the

weather station throughout the study had more variability than other ambient variables and were not normally distributed. This was because observations were recorded 24 hours per day and solar radiation values were 0 Watt/m^2 during night hours. Equation 3.1 was used in the calculation of the modified Z-score and all solar radiation values with an absolute modified Z-score greater than 3.5 were removed from the study (Iglewicz and Hoaglin, 1993). This method was applied to this study using Microsoft Excel functions.

$$M_i = \frac{0.6745(X_i - \tilde{X})}{MAD} \tag{3.1}$$

where,

M_i = Modified Z-Score

X_i = Observation

$\tilde{X}$ = Median of Observations

MAD = The Median Absolute Deviation of the Dataset

3.6.3 Development of Multiple Linear Regression Models

To create MLR models, a Repeated Random Sub-Sampling Validation (RRSSV; also known as Monte Carlo-Cross Validation) algorithm was developed and applied to each MLR model. MLR models used Ambient Variables to estimate a value for a specific Sensor Variable. RRSSV is an interactive cross-validation method which, under each iteration, randomly partitions available data into a training dataset and a testing dataset. The training dataset was used to create, or train, a data-driven model, which was then applied to the testing observations to estimate their corresponding values for the dependent variable. Then, a comparison between estimated and actual values of the dependent variable was used to determine the accuracy and reliability of the model. The algorithm

implemented randomly selected 80% of the observations to be used for training the model and the remaining 20% was reserved for testing.

An MLR model was developed for each combination of Ambient Variables under each of the 100 iterations and for each sensor variable. The five Ambient Variables could be combined in 31 different ways. Across 100 iterations this resulted in 3,100 different MLR models per Sensor Variable. Including all 10 Sensor Variables, a total of 31,000 MLR models were developed and analyzed. Listed below are the 31 different combinations of ambient variables analyzed in the study.

Models with one Independent Variable:

- $T = b_0 + b_1 X_1$
- $T = b_0 + b_2 X_2$
- $T = b_0 + b_3 X_3$
- $T = b_0 + b_4 X_4$
- $T = b_0 + b_5 X_5$

Models with two Independent Variables:

- $T = b_0 + b_1 X_1 + b_2 X_2$
- $T = b_0 + b_1 X_1 + b_3 X_3$
- $T = b_0 + b_1 X_1 + b_4 X_4$
- $T = b_0 + b_1 X_1 + b_5 X_5$

- $T = b_0 + b_2X_2 + b_3X_3$
- $T = b_0 + b_2X_2 + b_4X_4$
- $T = b_0 + b_2X_2 + b_5X_5$
- $T = b_0 + b_3X_3 + b_4X_4$
- $T = b_0 + b_3X_3 + b_5X_5$
- $T = b_0 + b_4X_4 + b_5X_5$

Models with three Independent Variables:

- $T = b_0 + b_1X_1 + b_2X_2 + b_3X_3$
- $T = b_0 + b_1X_1 + b_2X_2 + b_4X_4$
- $T = b_0 + b_1X_1 + b_2X_2 + b_5X_5$
- $T = b_0 + b_1X_1 + b_3X_3 + b_4X_4$
- $T = b_0 + b_1X_1 + b_3X_3 + b_5X_5$
- $T = b_0 + b_1X_1 + b_4X_4 + b_5X_5$
- $T = b_0 + b_2X_2 + b_3X_3 + b_4X_4$
- $T = b_0 + b_2X_2 + b_3X_3 + b_5X_5$
- $T = b_0 + b_2X_2 + b_4X_4 + b_5X_5$
- $T = b_0 + b_3X_3 + b_4X_4 + b_5X_5$

Models with four Independent Variables:

- $T = b_0 + b_1X_1 + b_2X_2 + b_3X_3 + b_4X_4$
- $T = b_0 + b_1X_1 + b_2X_2 + b_3X_3 + b_5X_5$
- $T = b_0 + b_1X_1 + b_2X_2 + b_4X_4 + b_5X_5$
- $T = b_0 + b_1X_1 + b_3X_3 + b_4X_4 + b_5X_5$
- $T = b_0 + b_2X_2 + b_3X_3 + b_4X_4 + b_5X_5$

Models with five Independent Variables:

- $T = b_0 + b_1X_1 + b_2X_2 + b_3X_3 + b_4X_4 + b_5X_5$

3.6.4 Algorithm Process

The algorithm explained above was run for each Sensor Variable, following the five-step process below:

1. Extracted observations that contained recorded values for all Ambient Variables and for the Sensor Variable under consideration. Due to missing and discarded outlying values, not all observations had values for all Ambient and Sensor Variables. Therefore, not all models were created with the same number of observations. Table 3 shows the number of observations (N) used in the modeling of each Sensor Variable, as well as the respective sizes of the training (m) and testing (p) datasets.

Table 3 Size of Random Data Partitions

Sensor Location	Sensor Variable	Number of Observations (N)	Size of Training Dataset (m) (80%)	Size of Testing Dataset (p) (20%)
0 ft	Black_0 White_0	1,262	1,010	252
1 ft (0.30 m)	Black_1 White_1	1,398	1,118	280
2 ft (0.61 m)	Black_2 White_2	1,285	1,028	257
3 ft (0.91 m)	Black_3 White_3	1,284	1,027	257
4 ft (1.22 m)	Black_4 White_4	1,285	1,028	257

2. Developed the 100 random partitions with the available N observations.

3. For each partition:

    a. Developed 31 MLR models using the m observations in the training dataset.

    b. Each of the 31 models developed applied to observations in the testing dataset and calculated percent error per model for each observation as shown in Equation 3.2.

$$PE_{ijkl} = \frac{ET_{ijkl} - AT_{ij}}{AT_{ij}} \times 100\% \quad (3.2)$$

where,

PE_{ijkl} = Percent Error for Sensor Variable i (each of the 10 Sensor Variables) at Testing Observation j (1 to m) for iteration l (1 to 100) using model k (1 to 31)

ET_{ijkl} = Estimated Temperature for Sensor Variable i at Testing Observation j for iteration l using model k

AT_{ij} = Actual Temperature for Sensor Variable i at Testing Observation j

c. Calculated Mean Absolute Percentage Error (MAPE) value for each of the 31 models developed for each sensor within each of the 100 iterations using Equation 3.3.

$$MAPE_{ijkl} = \frac{\sum_1^j |ET_{ijkl}|}{m_i} \times 100\% \quad (3.3)$$

where,

$MAPE_{ijkl}$ = Mean Absolute Percentage Error for Sensor Variable i (each of the 10 Sensor Variables) for iteration l (1 to 100) using model k (1 to 31)

ET_{ijkl} = Estimated Temperature for Sensor Variable i at Testing Observation j for iteration l using model k

m_i = Size of Testing Dataset for Sensor Variable i

4. Calculated the mean of the Sampling Distribution created with the 100 MAPE values calculated for each MLR model. The mean value of the Sampling Distribution approximated the population MAPE. Population MAPE in this study refers to the population of percent errors expected for a given MLR model.

5. Analyzed results from the MAPE Sampling Distribution to:

    a. Identify patterns in performance of the Ambient Variables as MLR inputs across all Sensor Variables.

    b. Identify Ambient Variables that offered the best performance (lowest population MAPE) and defined the final MLR model with those variables using the sampling distribution of the regression coefficients across 100 random partitions. Then, used those MLR models to develop temperature profiles for both experimental decks.

    c. Identify and develop more practical models that offered comparable performance with less Ambient Variables that were more accessible by intended model users. Levene's and ANOVA test loops, as described by Pakalapati (2018), were applied to determine if there were more practical models with statistically similar performance as the best model identified for each Sensor Variable.

CHAPTER FOUR: ANALYSIS OF RESULTS

4.1 ANALYSIS OF MLR MODELS

Figure 8 shows an example of population MAPE values for the Sensor Variable installed 1 foot above the white surface (White_1). MAPE values were sorted in ascending order, showing that the MLR model created with all five Ambient Variables offered the best overall accuracy and reliability. Population MAPE values for all Sensor Variables showed a similar distribution as the one shown in Figure 8, except the MAPE values for temperate estimates at the black surface (Black_0). For all other Sensor Variables, population MAPE values were divided into the same four groups shown in Figure 8.

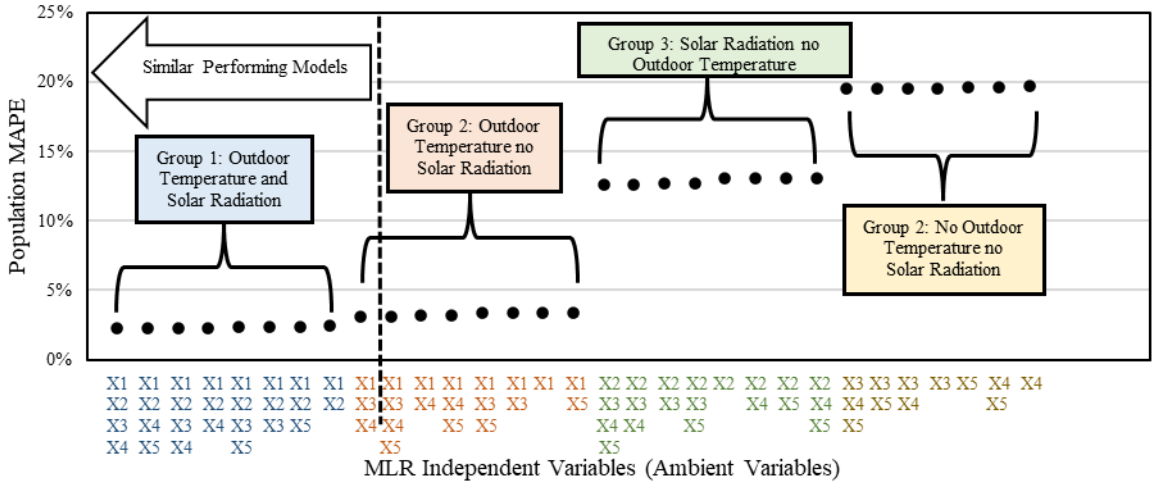

Figure 8 Sorted Population MAPE Values for Sensor Variable White_1.

The order of models could have changed within each group, but the groups always appeared in the same order, with the eight models that included Outdoor Temperature (X1) and Solar Radiation (X2) Variables, showing the best overall performance (Group 1). They were closely followed by the remaining eight models that used Outdoor Temperature but not Solar Radiation (Group 2). There was a clear difference in performance of those models using Solar Radiation but

not Outdoor Temperature (Group 3). The next group (Group 4) consisted of the MLR models that offered the worst performance, which were the models that do not use Outdoor Temperature or Solar Radiation as independent variables. The main difference between the Black_0 Sensor Variable and the other variables was Group 2 was split into two parts. The level of performance of the first four models in Group 2 was at the midpoint of the gap between Groups 1 and 3. The performance of the other four models of Group 2 was at the same level of Group 3, overlapping with the first few models of that group.

The order of the groups confirmed the statement made before that Outdoor Temperature and Solar Radiation variables offered the highest accuracy and reliability among other models. Removing the Solar Radiation variable slightly increased population MAPE values. Figure 9 shows the same MAPE values for Groups 1 and 2 but increasing the scale of the vertical axis to better see the difference between these two groups.

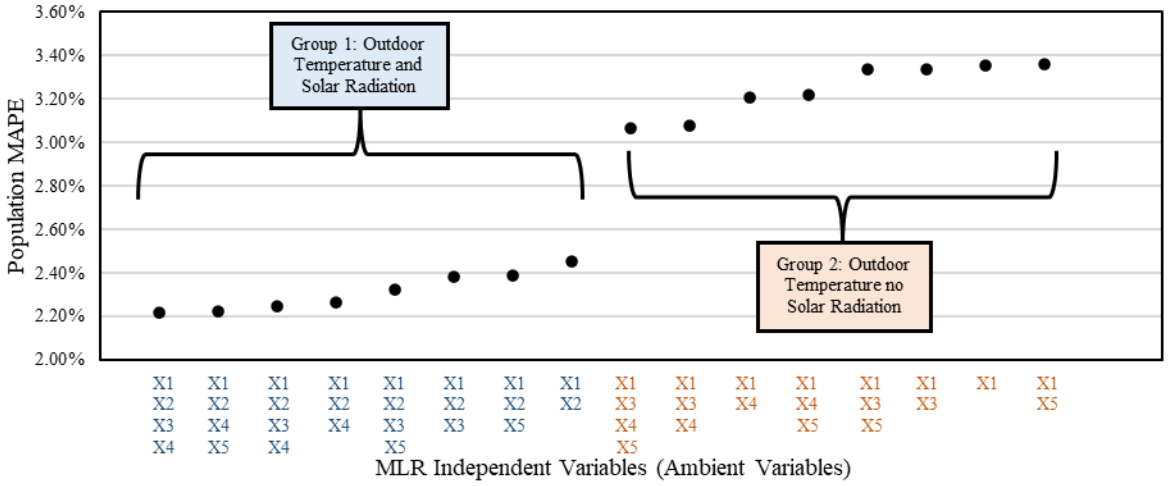

Figure 9 Sorted Population MAPE Values for Sensor Variable White_1: Groups 1 and 2.

Performance reduction was greater when the Outdoor Temperature variable was removed instead of Solar Radiation, confirming that Outdoor Temperature was the most relevant independent variable. This was expected because of the significant variability of solar radiation

values. Cloudy days and clouds passing in front of the sun for short periods of time resulted in sudden decreases and increases in solar radiation values. Relevance of the different independent variables was also assessed via statistical significance testing. An MLR model was created for each Sensor Variable, using all five Ambient Variables and all the available observations. A t-test was applied on the coefficient of each Ambient Variable to determine if they were statistically significant. Researchers typically use a 95% confidence level to determine whether an independent variable is statistically significant, which corresponds to a p-value lower than or equal to 0.05. Based on the p-values shown in Table 4 for all Ambient Variables in MLR models created for each Sensor Variable, it was possible to conclude with 99.9% confidence (p-value ≤ 0.001) that all five Ambient Variables, except Relative Pressure, were significant inputs for all MLR models. The Relative Pressure variable was no longer significant at some point between one and two feet above the black surface. That means this variable was not statistically significant for the MLR models for Black_2, Black_3, and Black_4. Relative Pressure was statistically significant for all Sensor Variables on the white deck.

Table 4 Multiple Linear Regression Coefficients with all Observations (N)

Sensor Variable	P-Value & Rank	Outdoor Temperature	Solar Radiation	Outdoor Humidity	Relative Pressure	Wind Speed
Black_0	P-value	0.00	1.8E-167	2.9E-58	1.6E-11	1.4E-16
	Rank	1	2	3	5	4
Black_1	P-value	0.00	3.3E-82	3.0E-05	3.1E-20	1.3E-07
	Rank	1	2	5	3	4
Black_2	P-value	0.00	9.6E-91	2.0E-24	0.6528	1.5E-15
	Rank	1	2	3	5	4
Black_3	P-value	0.00	7.2E-65	2.0E-26	0.8271	1.4E-15
	Rank	1	2	3	5	4
Black_4	P-value	0.00	3.4E-49	5.6E-23	0.3656	4.1E-14
	Rank	1	2	3	5	4
White_0	P-value	0.00	3.6E-152	4.6E-36	5.9E-25	1.1E-11
	Rank	1	2	3	4	5
White_1	P-value	0.00	6.7E-192	5.7E-06	1.3E-32	4.6E-10
	Rank	1	2	5	3	4
White_2	P-value	0.00	5.8E-142	5.8E-28	2.7E-04	4.2E-19
	Rank	1	2	3	5	4
White_3	P-value	0.00	2.3E-130	1.6E-13	1.3E-34	1.2E-20
	Rank	1	2	5	3	4
White_4	P-value	0.00	7.4E-127	1.3E-29	1.3E-08	1.2E-17
	Rank	1	2	3	5	4

Statistical significance of all Ambient Variables as inputs for a given MLR model did not necessarily mean that the best possible MLR for the intended Sensor Variable should have included all those variables. Less variables could have offered better performance during the implementation of the model with new data not used for model development. The RRSSV algorithm developed in this study was intended to rank the performance of different independent variable combinations by testing them in an iterative manner against a testing dataset. Models were ranked according to their population MAPE values.

Table 5 shows the Ambient Variables of the top ranked MLR models identified through Levene's and ANOVA testing. According to these statistical tests, the MLR models showed a comparable performance with a homogenous variance (Levene's test) and similar average accuracy (ANOVA test) with a 95% confidence level. Apart from Black_0 Sensor Variable, top ranked MLR models for all Sensor Variables included all Group 1 models. Top models for Black_1

and Black_4 also included all Group 2 models, while models for Black_2 and Black_3 only included the first four and five models, respectively, of Group 2. The Black_0 variable is the only one with four models that showed a top comparable performance. Top ranked models for the five Sensor Variables in the white deck were more limited to the first group, with one the first model of Group 2 barely joining the top group of models for White_1 and White_3. The nine top models for White_1 are also shown in Table 5.

Table 5 Top Ranked MLR Models for Each Sensor

Black_0	Black_1	Black_2	Black_3	Black_4
1. X1 X2 X3 X4	1. X1 X2 X3 X4 X5	1. X1 X2 X3 X5	1. X1 X2 X3 X5	1. X1 X2 X3 X5
2. X1 X2 X3 X4 X5	2. X1 X2 X4 X5	2. X1 X2 X3 X4 X5	2. X1 X2 X3 X4 X5	2. X1 X2 X3 X4 X5
3. X1 X2 X3 X5	3. X1 X2 X3 X4	3. X1 X2 X3	3. X1 X2 X3	3. X1 X2 X3
4. X1 X2 X3	4. X1 X2 X4	4. X1 X2 X3 X4	4. X1 X2 X3 X4	4. X1 X2 X3 X4
5. X1 X2	5. X1 X2 X3 X5	5. X1 X2 X4 X5	5. X1 X2 X4 X5	5. X1 X2 X4 X5
	6. X1 X2 X3	6. X1 X2 X4	6. X1 X2 X5	6. X1 X2 X5
	7. X1 X2 X5	7. X1 X2 X5	7. X1 X2 X4	7. X1 X2 X4
	8. X1 X2	8. X1 X2	8. X1 X2	8. X1 X2
	9. X1 X3 X4	9. X1 X3 X4 X5	9. X1 X3 X4 X5	9. X1 X3 X5
	10. X1 X3 X4 X5	10. X1 X3 X4	10. X1 X3 X5	10. X1 X3 X4 X5
	11. X1 X4	11. X1 X3 X5	11. X1 X3 X4	11. X1 X3 X4
	12. X1 X4 X5	12. X1 X3	12. X1 X3	12. X1 X3
	13. X1 X5		13. X1 X4 X5	13. X1 X4 X5
	14. X1			14. X1 X4
	15. X1 X3 X5			15. X1 X5
	16. X1 X3			16. X1
White_0	White_1	White_2	White_3	White_4
1. X1 X2 X3 X4	1. X1 X2 X3 X4 X5	1. X1 X2 X3 X5	1. X1 X2 X3 X4 X5	1. X1 X2 X3 X4 X5
2. X1 X2 X3 X4 X5	2. X1 X2 X4 X5	2. X1 X2 X3 X4 X5	2. X1 X2 X4 X5	2. X1 X2 X3 X5
3. X1 X2 X3	3. X1 X2 X3 X4	3. X1 X2 X3	3. X1 X2 X5	3. X1 X2 X3 X4
4. X1 X2 X3 X5	4. X1 X2 X4	4. X1 X2 X3 X4	4. X1 X2 X3 X4	4. X1 X2 X3
5. X1 X2 X4	5. X1 X2 X3 X5	5. X1 X2 X4 X5	5. X1 X2 X3 X5	5. X1 X2 X5
6. X1 X2 X4 X5	6. X1 X2 X3	6. X1 X2 X5	6. X1 X2 X4	6. X1 X2 X4 X5
7. X1 X2	7. X1 X2 X5	7. X1 X2 X4	7. X1 X2	7. X1 X2
8. X1 X2 X5	8. X1 X2	8. X1 X2	8. X1 X2 X3	8. X1 X2 X4
	9. X1 X3 X4		9. X1 X3 X4 X5	

4.2 DETERMINATION OF MLR EQUATION

Having identified the best model (lowest population MAPE) for each Sensor Variable, the next step was to determine the final coefficients for each model. Rather than finding the best set

of coefficients for each Sensor Variable, the RRSSV algorithm best aimed to identify the set of Ambient Variables that could better explain the temperatures recorded by each Sensor Variable. The RRSSV algorithm provided 100 sets of coefficients for each combination of independent variables resulting in one set of coefficients for each random partition. Each regression coefficient in the final MLR model was defined as the average of its corresponding sampling distribution formed by the 100 regression coefficients. Those average values were assumed to be a better representation of actual population coefficients. Resampling and sampling distributions are commonly used in research to understand the variability in regression coefficients (de Bin et al., 2016; Dixon, 2001; Schumacher, 1992) given that MLR models are developed with samples rather than with an entire population.

Table 6 shows the final regression coefficients for the top MLR model for each Sensor Variable, which were used to develop temperature profiles for each experimental deck based on local climate conditions. Temperature profiles in Figure 10 were calculated with average climate conditions recorded at the experiment location during the dates and times of the final dataset used for the analysis in this study.

Table 6 Final Multiple Linear Regression Coefficients

Sensor Variable	Regression Coefficients					
	b_0	b_1	b_2	b_3	b_4	b_5
Black_0	170.360	1.230	0.036075	-0.256	-5.429	N/A
Black_1	40.503	1.024	0.004787	0.013	-1.434	-0.131
Black_2	0.421	1.001	0.004519	-0.028	N/A	-0.163
Black_3	3.807	0.976	0.003729	-0.030	N/A	-0.165
Black_4	4.997	0.975	0.003156	-0.029	N/A	-0.155
White_0	147.720	1.086	0.020323	-0.117	-4.933	N/A
White_1	73.045	1.042	0.011380	0.019	-2.616	-0.220
White_2	3.493	1.001	0.011312	-0.050	N/A	-0.349
White_3	91.307	1.072	0.010042	-0.037	-3.155	-0.344
White_4	45.736	1.035	0.010185	-0.059	-1.474	-0.327

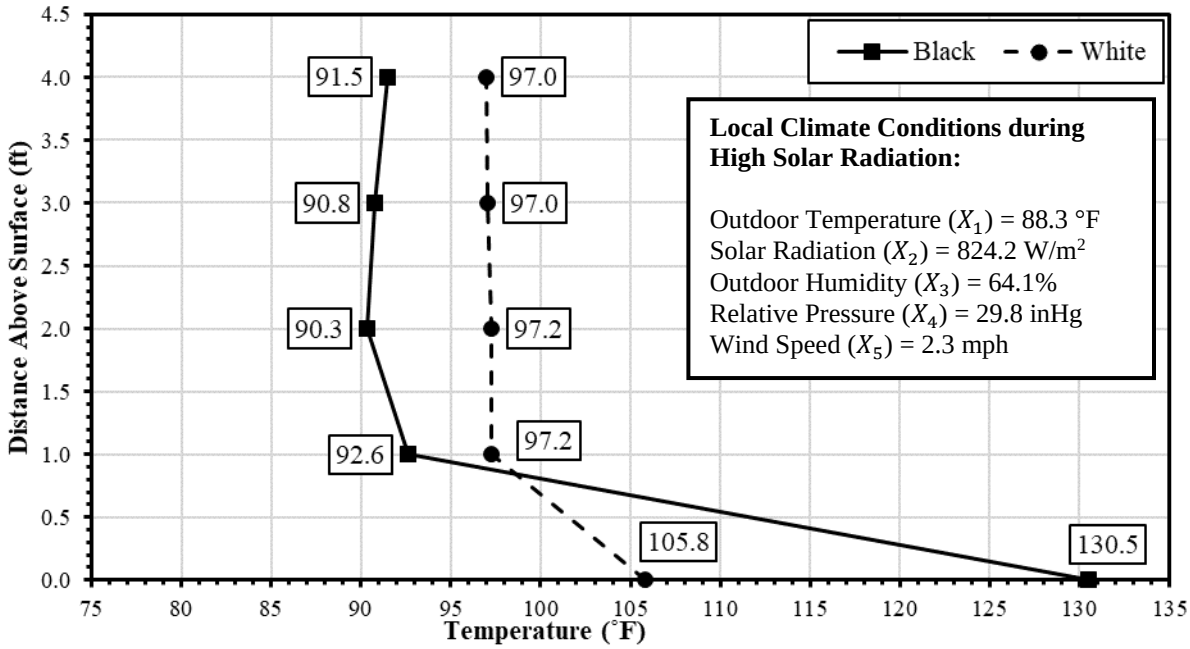

Figure 10 Temperature Profiles for Decks at Experiment Site (Opelika, AL).

4.3 SUMMARY

This chapter provided the testing results for evaluating the effects of reflectivity on air and surface temperatures up to 4 ft (1.22 m) above the roof surface. Multiple linear regression was used to create the final model and parameters were selected based on reliability and significance of the ambient variables recorded by the weather station. Also, the ambient variables selected needed be practical for the user to easily access. An extensive analysis was conducted to clean the data and create random sampling distributions to determine the final coefficients for the MLR equation. The development of this data analysis process and MLR model provided performance evaluations and empirical results to the cool roof industry in future testing efforts. Additionally, the final model will provide designers with a useful tool to predict above-roof temperatures when considering roof materials.

CHAPTER FIVE: DISCUSSION AND RECOMMENDATIONS

5.1 ABOVE SURFACE AIR TEMEPRATURE

The results presented in the analyses above were important in determining the effectiveness of the roofing material selected on overall building energy efficiency. In the final temperature profiles for the white and black decks, using average ambient conditions from testing dates, there were temperature differences in the decks of nearly 6 to 7˚F (3.3 to 3.9˚C) while 2 to 3 ft (0.61 to 0.91 m) above the decks. On average, temperature was 5.8˚F (3.2˚C) higher above the white deck than the black deck. Also, temperatures above the white deck surface were, on average, 8.8˚F (4.9˚C) higher than ambient outdoor temperature compared to 3.0˚F (1.7˚C) for the black deck. This resulted in a 10.0% increase from ambient temperature above the white deck and an increase in 3.4% for the black deck. These temperature increases can result in significantly higher energy consumption of an HVAC unit than estimated with BPS practices.

It is important that roofing insulation, roofing membrane, and above surface conditions are all considered when determining the most effective way to decrease energy consumption. Studies have shown that on a global scale, cool roofing increased heating costs more than they decreased cooling costs on an annual average, rendering them ineffective in certain climates (Oleson et al., 2010). Thus, a cool roof should be selected based on the building's geographical location and not on the theory of a cool roof being the universal fix for energy savings.

Although this study was conducted in Opelika, Alabama, a warm southern climate, testing was conducted from July until December to have a wider range of ambient temperatures to test. Results could vary based on geographic location due to changes in the Ambient Variables used in this study. At higher latitudes, not only do ambient temperatures decrease, but variables such as

solar radiation will change as well because of a change in solar elevation. These are all factors to include when considering climate. A limitation of this study was being confined to one location for testing. Future studies should consider experimental testing or monitoring in multiple climate regions.

5.2 ROOF AND ADJACENT SURFACE TEMPERATURE

As expected, surface temperatures of the black deck were significantly higher than the white deck. The surface of the white roofing membrane is much cooler and will reduce heat flux into the building. Under the conditions presented in the final model, the black EPDM membrane reached 130.5˚F (54.7˚C) and the white PVC membrane reached 105.8˚F (41˚C). This corresponded with a 47.8% and 19.8% increase in temperature from an ambient temperature of 88.3˚F (31.3˚C), respectively. Reduced temperature of the white membrane is ideal in warm environments for mitigating heat transfer through the roofing assembly, but potential drawbacks should be considered. Unintended consequences of reflectivity of the white membrane could be damage to surrounding rooftop equipment, materials, and adjacent surfaces. Equipment such as HVAC units and photovoltaic (PV) panels can suffer from exposure to high intensity of solar radiation for long durations. Degradation of common rooftop materials like flashing and caulking can be accelerated from exposure to incoming and reflected solar radiation.

The efficiency of PV panels decreases when operating at higher temperatures. Even if the PV panel is mounted just one foot above the cool roof surface, this study has shown that temperatures can be increased significantly at that height. Roof flashings often terminate within a few inches of the surface at adjacent walls. This termination sometimes relies on caulking to remain watertight. These products typically will degrade faster at higher temperatures. Flashing

at roof parapets is exposed to higher temperatures from reflected infrared radiation. This will age the material faster than the roof surface.

In this study, surface temperatures of the white membrane were lower than ambient temperature at night and at some points during the day in colder months. This causes condensation to form on and under the membrane. Condensation is a potentially destructive consequence that is unintended with cool roofing (Ibrahim, 2013-1). In below-freezing temperatures, condensation will turn into frost and ice, potentially damaging the roof assembly. Also, unwanted effects such as molding around rooftop equipment and materials can occur. Even during this study, it was observed that mold began to form around equipment on the white deck. Over the course of a cool roof's lifetime, these effects from condensation can become more prominent.

Other potential consequences from lower surface temperatures of a cool roof to consider are loss of membrane adhesion, damage to roofing assembly and insulation, and leakage through the roof. Over time, condensation will continue to accumulate on and under the roof surface, causing the adhesion of the membrane to reduce. If not properly maintained, cool roof membranes can become detached due to loss of adhesion and wind forces. Condensation can also create problems for roof assembly materials such as plywood and insulation. When subjected to moisture, these items can deteriorate over time and be prone to molding. Finally, increased condensation can cause leaks and drips to begin to form through the roof due to the deterioration of the roof assembly. It is recommended that corrosion and deterioration of rooftop equipment, materials, and the rooftop assembly due to increased condensation are investigated in future studies. This would further knowledge of benefits and drawbacks of cool roofs and help develop proper selection and maintenance practices.

5.3 INSTRUMENTATION

Another recommendation is that future testing should experiment with multiple instrumentation devices for measuring surface and air temperature. In this study, temperature sensors recording air temperature above each deck were partially shielded. This means that sensors were completely shielded from incoming solar radiation, but not completely shielded from solar radiation reflected from the deck. Instead of traditional radiation shields, the 90˚ downward PVC elbow served as a means of protecting the temperature sensor from as much solar radiation as possible. Similar studies have recorded air temperature with fully shielded, partially shielded, and unshielded sensors (Grant et al., 2017; Green et al., 2020; Ibrahim, 2013-2; Wray & Akbari, 2008).

Radiation shields are used to prevent the temperature sensor from being affected by incoming or reflected solar radiation, but it is possible that the shield itself is affecting temperature readings when dealing with such minor differences in temperature. Previous studies used different methods and products when it comes to shielding temperature sensors It is challenging to draw comparisons between the results of this study and those from prior studies because of differences in climate conditions, buildings, roofing materials, and instrumentation. It is recommended that further experimentation be conducted on different methods of instrumentation selection and configuration prior to implementing them into a future study.

5.4 ROOFTOP EQUIPMENT

Fresh air intakes on most HVAC units mounted on rooftops are within 4 ft (1.22 m) of the roof surface. The intent of a cool roof is to lower the surface temperature and heat transferred into the building, but if the air entering the intake is warmer than ambient temperature then the HVAC unit would be using more energy to cool the air. Energy calculators are used to determine building energy efficiency through simulation. The simulations typically assume that HVAC equipment is

subjected to outdoor ambient air temperature obtained by a weather file (Green et al., 2020). The environment above the roof surface is different than ambient conditions. This would lead to errors in energy savings predicted by simulations when comparing cool roof options.

5.5 POSSIBLE SOLUTIONS

To mitigate energy losses of rooftop equipment and slow degradation of materials on a roof, the rooftop environment must be considered to implement viable solutions. For example, a building in a cold climate zone, where there are more days of cold weather than warm weather, might benefit from a darker color roofing membrane than a highly reflective membrane. In a cold climate zone, a reflective membrane will be much cooler than a dark membrane on the surface and will be more susceptible to accumulating condensation. The reflective membrane will not dry as easily in cold temperatures and will result in more molding on roof surfaces and rooftop equipment, along with other consequences as described previously. In hot climates, like the climate for this study, a reflective roofing membrane is going to be a superior choice to a dark, non-reflective, membrane due to extremely high surface temperatures of the darker membrane or coating, but deficiencies should be considered. If surrounding air and surface temperatures are being increased due to reflectivity, then energy savings may not be as high as expected.

For this study, the adjacent wall for both decks were facing directly south, which subjects the wall surface to the most extreme conditions. On a southern facing parapet wall of a roof, a less reflective material should be considered. The increased reflectivity of the flashing will increase temperatures of nearby air and surface temperatures and accelerate degradation of caulking which provides the water-tight seal of the membrane. This would help decrease maintenance costs and the amount of cleaning needed for the roof. For rooftop equipment such as HVAC units and PV panels, efficiency could be improved by implementing certain practices into standards. In hot

climates, an HVAC unit could be mounted over a less reflective material to reduce the intensity of solar radiation reflected onto the unit. This study proved air temperature could be nearly 10°F (5.56˚C) above ambient temperature and surrounding surface temperatures are significantly increased up to 4 ft above the roof surface. This is the height where most air intakes are located on an HVAC unit. If an HVAC unit was mounted over a less reflective material with a dull finish, air temperature could be significantly decreased, as well as the surface temperature of the unit itself. This can also be applied to PV panels mounted on rooftops. Mounting over less reflective surfaces or elevating to heights above 4 ft (1.22 m) could improve efficiency. Also mounting over a less reflective surface or elevating could protect rooftop equipment from degrading by effects of reflected solar radiation or roof condensation.

5.6 FUTURE RESEARCH

It is recommended that this study is continued to further knowledge of the impacts of roof material and color on above-roof air and surface temperatures. As stated previously, it is particularly important that future studies experiment with various products and configurations of temperature sensors. Studies should investigate with fully shielded and partially shielded sensors, as well as experiment with several types of sensors. Additionally, the effects of fan-aspirated radiation shields on temperature sensors should be examined. This step should be completed first and is important because it is necessary in the process to ensure accurate data collection.

Studies should propose large-scale empirical studies that are designed to overcome limitations in this research and previous studies. This study conducted tests on small-scale constructed decks where roofing material and data collection strategies were controlled. Previous studies conducted tests on large buildings with low-sloped roofs where roofing materials and experimental design was dependent on the building’s rooftop configuration. To best evaluate and

compare cool and traditional low-reflectance roofs, testing should be conducted on experimental buildings which are designed and controlled by the research team and subjected to real-world conditions.

The proposed future research should monitor ambient and above-roof temperatures, HVAC energy consumption, moisture accumulated in the roof assembly, and material deterioration over time. The roof assembly and walls should be constructed to standards commonly used in large buildings with low-sloped roofs. Additionally, indoor conditions should be controlled to monitor HVAC unit energy consumption. This study should also implement different strategies to optimize building energy consumption and reduce material degradation. Strategies should include improved design and placement of HVAC units to minimize energy consumption by strategically positioning fresh air intakes in areas with favorable temperatures. An empirical study of this scale, and with this amount of control, under real-world conditions would remove any limitations experienced in this thesis research or previous studies examined.

CHAPTER SIX: CONCLUSIONS

With an increase in the use of light-colored, reflective, roofing membranes, building owners and contractors have continued to neglect real world applications and considering the configuration of the rooftop as a whole. Cool roofs have been implemented into most building codes to satisfy green initiatives. Although studies on the benefits of cool roofs are extensive, little attention has been given to the possible adverse effects of their usage. Current BPS practices depict large savings on energy costs, but do not consider the effects that reflectivity have on above-roof conditions.

On traditional low-reflectance roof coatings and membranes, incoming solar energy is absorbed with little to no reflectance. In comparison, cool roofs reflect considerable amounts of solar energy that heats the surrounding air and nearby surfaces. While lower surface temperatures can decrease heat flux into the building interior, potential increases or decreases in air and surface temperatures up to 4 ft (1.22 m) can affect energy use of rooftop equipment and accelerate aging and degradation of common rooftop materials. Building performance simulations traditionally use local ambient temperatures to model HVAC fresh air intake temperature. Reported energy savings by these simulations are limited by the ability to consider real-world complexities of the rooftop environment.

This study consisted of a comprehensive literature review to investigate potential benefits and drawbacks of cool roofs, experimental design testing of roofing materials, and an extensive data analysis to determine the effects of reflectivity up to 4 ft (1.22 m) above the roof surface. Preliminary analyses revealed that reflectivity of the white membrane influenced air and adjacent surface temperatures up to 4 ft (1.22 m) above the experimental decks. In a test conducted on a sunny day, August 12, 2020, air temperature above the white membrane reached approximately

10˚F (5.56˚C) higher than ambient temperature and approximately 5˚F (2.78˚C) above the black membrane. Additionally, surface temperatures of the adjacent wall were higher above the black membrane than the black. These findings were a crucial step in discovering trends to develop the final model.

To create the final model to estimate surface and air temperatures up to 4 ft (1.22 m) above the white and black membranes, experiments were conducted from July to December of 2020. Averaging ambient conditions from the final dataset resulted in an outdoor temperature of 88.3˚F (31.3˚C), solar radiation of 824.2 W/m^2, outdoor humidity of 64.1%, relative pressure of 29.8 inHg (100.9 kPa), and a wind speed of 2.3 mph (1.03 m/s). These five ambient conditions were used as independent variables in the best performing multiple linear regression equation to estimate surface temperature and air temperature up to 4 ft (1.22 m) above the rooftop. The final model estimated a 47.8% and 19.8% increase in surface temperature from average ambient temperature for the black and white membranes, respectively. Temperatures up to 4 ft (1.22 m) above the white membrane were increased 10.0% from average ambient outdoor temperature. Additionally, temperatures up to 4 ft (1.22 m) above the black membrane were higher than average ambient temperature by 3.4%.

Testing in different climate zones would be beneficial to understand how factors such as humidity and solar elevation affect the rooftop environment. This study has shown that temperatures above reflective and non-reflective materials can be higher than ambient outdoor temperature up to 4 ft (1.22 m) above the surface, so further research on the efficiency on an HVAC unit or PV panels would help validate the importance of this study. Future studies should identify temperature ranges where rooftop equipment efficiency could be optimized. For example, in colder climates it could be more cost effective to use a non-reflective membrane and improve roofing

insulation rather than an increase in energy consumption by rooftop mechanical systems. Further research described above would continue discussions on how there are several options for improving rooftop conditions and increasing building efficiency, and not just a simple, singular, choice to satisfy a green initiative.

PART TWO: EVALUATION OF SURFACE SKIMMER FLOW RATES AND SIZE SELECTION

ABSTRACT

A floating surface skimmer is a device used to dewater a sediment basin as it fills. The skimmer floats on the surface, draining the least turbid water as sediment falls out of suspension. An adjustable orifice on the skimmer helps to regulate the filling and draining rate of the basin. After significant runoff events, skimmers will slowly drain the basin over several days to maximize settling, while draining less turbid water from the top of the water column . Since water typically enters a sediment basin at a higher flow rate than the skimmer removes the water, soil particles can settle to the bottom of the basin. There are several options when choosing a skimmer product. Manufacturers have published data for their products that customers can use to decide on skimmer type, size, and orifice opening, but these design parameters tend to be very rough estimates with numerous assumptions. This research details a methodology for testing skimmers including materials, data collection process, and data analysis approach.

In addition, testing was performed in a 7 ft (2.13 m) deep evaluation tank with a volume of approximately 1,000 ft^3 (30 m^3). The skimmer tested was a 6-in. (15.2 cm) post-construction stormwater prototype provided by J.W. Faircloth & Son, Inc. which used an adjustable sluice gate to create openings from 0.5 to 6.0-in. (1.3 to 15 cm) in 0.5-in. (1.3 cm) increments. The skimmer was attached to the discharge outlet of the testing tank which discharges to a nearby pond. A constructed water delivery system was used to fill the tank and a Solinst Levelogger® recorded water levels in 5 sec. intervals as the skimmer dewatered the tank. This process was repeated 36 times with varying barrel lengths and sluice gate openings, with each setting having triplicate tests performed. Experiments revealed that the skimmer had a capacity of 0.5 ft^3/s (0.03 m^3/s) with a 1.0-in. (2.5 cm) and a capacity of 2.5-3.0 ft^3/s (0.071-0.085 m^3/s) with an opening of 6.0-in. (15 cm).

Results from these experiments were used to develop models to approximate the flow rate of the skimmer at various water depths. These models were then used to create a user-interactive skimmer sizing tool in Microsoft Excel. The user inputs values such as basin elevations and cross section properties to calculate the basin volume. The user can then select the number of skimmers and the opening sizes to obtain data and graphs on flow rates at each depth, basin storage, and the total design drawdown time. This method of testing and data analysis is more thorough than present practices in the industry and provides designers with more accurate information on sediment basin storage and drawdown times based on skimmer selection.

CHAPTER SEVEN: INTRODUCTION

7.1 BACKGROUND

The construction industry is one of the leading causes of sediment-laden stormwater runoff in the United States. Construction activities such as land clearing, excavating, and grading expose underlying soil to erosion forces (Fang et al., 2015). Erosive forces may transport exposed soils to waterways where they are eventually deposited. Construction sites can deposit more sediment into waterways in a short period of time than can be deposited naturally over decades (Environmental Protection Agency [EPA], 2000). Sediment runoff rates on construction sites ae typically 10 to 20 times greater than runoff from agricultural lands and 1,000 to 2,000 times greater than those of forest lands (EPA, 2000). This results in estimated erosion rates of 20 to 200 tons per acre (448 tonnes per hectare) per year from construction sites (Pitt et al., 2007). Sediment-laden runoff from construction sites facilitates negative environmental impacts to receiving waterbodies and drastically affect water quality.

Regulations at federal, state, and local levels require that stormwater is controlled on-site, preventing construction generated pollutants from entering waterways (Perez, 2014). Stormwater runoff is controlled through the installation of various types of temporary erosion and sediment control techniques and best management practices (BMPs).

7.2 SEDIMENT BASINS

One form of a temporary erosion and sediment control practice commonly found on a construction site is a sediment basin. Sediment basins are used as a sediment-control technique to capture, temporarily detain, and treat sediment-laden stormwater prior to discharging to a natural waterway (Perez et al., 2016). Sediment basins are utilized to allow temporarily detained

stormwater time for sedimentation to occur. Sedimentation occurs through the settling of soil particles due to gravitational forces. Sediment basin designs and practices aim towards achieving the desired retention times required to remove as much sediment as possible from the effluent discharge. Government agencies provide standardized guidance for the design and BMPs associated with sediment basins on construction sites (ALDOT, 2020).

7.3 SEDIMENT BASIN DEWATERING

In addition to basin design requirements and sedimentation considerations, a form of dewatering the basin is necessary to remove treated stormwater and prevent extended ponding (Thaxton et al., 2004). Dewatering of a sediment basin is the process of slowly discharging stormwater runoff from the basin after detention time is achieved. Therefore, sediment basins must find a balance between allowing enough detention time for sediment to fall out of suspension while also maintaining enough available storage for future rainfall events. Dewatering of basins has traditionally been controlled with perforated riser structures, auxiliary spillways, and floating surface skimmers (Perez et al., 2018). Floating surface skimmers are becoming increasingly more popular with new designs and improvements to decrease turbidity and suspended solids in the effluent discharge. Proper sizing of skimmers allows a more efficient combination of clean discharge effluent and available storage than traditional dewatering methods.

7.4 FLOATING SURFACE SKIMMERS

Floating surface skimmers are used to drain water from the top of a water column in a basin, dewatering from the least turbid section of the basin. The skimmer floats on the surface, draining treated water as sediment falls out of suspension. The two main functions of a skimmer are to dewater the basin and reduce turbidity and suspended solids in the discharge. Traditionally, dewatering is achieved using riser pipes. Skimmers differ from riser pipes; in that they always

dewater the basin from the top where water is clearer. An adjustable orifice or sluice gate on the skimmer helps to regulate the filling and draining rate of the basin. On construction sites, basins are typically designed detain water for two to five days (AL-SWCC, 2018). Skimmers can also be used in permanent post-construction basins. Proper selection and sizing of skimmers is needed to meet sediment basin detention requirements.

Skimmer sizing is based on orifice or sluice gate opening size and basin dimensions. Detention requirements are met by combining basin dimensions with the skimmer size to achieve proper dewatering flow rates. Typically, skimmer flow rate requirements are determined by equations involving orifice diameter and basin volume or by experimental testing. Although these forms of skimmer sizing can often be relied upon for that specific skimmer product, research has shown that each product has its own hydraulic characteristics that affect flow rate (Sprague et al., 2015). Therefore, accurate discharge rates for each product must be determined through full scale experimental testing.

7.5 POST-CONSTRUCTION STORMWATER MANAGEMENT

Mitigation of stormwater runoff causing flood events is a primary concern for developed areas. Flood control measures typically depend on retention and detention of runoff from a significant storm event (Travis et al., 2008). Detention and retention basins are used to contain a storm event volume and obtain specific peak flow reductions, respectively. Detention basins temporarily reduce peak flow events to prevent receiving waters from exceeding capacity as well as remove pollutants. A retention basin's purpose is to hold a permanent storm event volume and establish vegetation to promote the settling of suspended solids. Developed, urban, areas cause major changes to the landscape by introducing large areas of impervious surfaces, changes in vegetation and soil permeability, changes in surface flow, and changes in groundwater flow

(Lawrence et al., 1996). These changes can significantly increase the runoff associated with storm events and the pollutants captured. Detention and retention basins can retain the on-site runoff of a watershed, but the main purpose of these basins is to reduce and delay peak runoff; not to capture and infiltrate stormwater runoff (Osouli et al., 2017).

There is an opportunity for floating surface skimmers to be used as a dewatering mechanism for post-construction detention and retention basins. Traditionally, permanent basins are dewatered by a spillway or riser structure. Skimmers are more effective at capturing suspended solids in the basin and allow for better control of available storage. This lends the opportunity for skimmers to be used in detention and retention basins for post-construction purposes as well.

7.6 RESEARCH OBJECTIVES

The objective of this research was to provide an accurate performance evaluation of the skimmer provided by J.W. Faircloth & Son, Inc. and enhance testing and data collection strategies. This research was divided into three primary components:

(1) Develop a full-scale testing method for evaluating the flow rate of a surface skimmer,

(2) Evaluate the skimmer using developed method through thorough data analyses, and

(3) Develop a final report with results that can be implemented for properly sizing surface skimmers.

The research project was divided into the following tasks to accomplish the objectives listed above:

(1) Develop and install modifications to existing skimmer evaluation tank at the Auburn University Stormwater Research Facility (AU-SRF),

(2) Develop falling head testing approach,

(3) Monitor flow rates using Teledyne Isco® 2150 Area Velocity Flow Module and Solinst Levelogger® 5,

(4) Develop a testing series that includes replicates and data analysis across various skimmer opening sizes,

(5) Develop performance graphs and flow rate curves for evaluated skimmer,

(6) Create a skimmer sizing tool to facilitate appropriate skimmer size selection,

(7) Develop a detailed summary of testing methodology including materials, data collection procedures, and data analysis approach, and

(8) Present performance of evaluated skimmer device.

7.7 EXPECTED OUTCOMES

The expected outcome of this research is to provide the erosion and sediment control industry knowledge and resources needed to accommodate growing regulations in stormwater management. Improved standards for evaluating surface skimmer flow rates for size selection will be realized through scientifically backed results. This research will provide an understanding of the importance of full-scale experimental testing and in-depth data analysis to achieve proper size selection to meet detention requirements. Furthermore, research efforts should stem from this project to grant future opportunities to expand knowledge of erosion and sediment control practices implemented on construction sites.

7.8 ORGANIZATION OF PART TWO

Part Two of the thesis is divided into five chapters that encompass the approach to meeting the defined research objectives. Following this chapter, Chapter Eight: *Literature Review*, provides an overview of current standards and practices used in skimmer evaluation. Chapter Nine: *Means and Methods*, outlines experimental design, procedures, data collection, and data analysis

developed to perform skimmer evaluations. Chapter Ten: *Results and Discussion*, presents the findings of experimental tests including data analyses and observations. Chapter Eleven: *Conclusions and Recommendations*, provides a comprehensive summary of the findings and recommendations on future research opportunities to advance this topic.

CHAPTER EIGHT: LITERATURE REVIEW

8.1 SEDIMENT BASIN DEWATERING

8.1.1 Riser Structure

Traditionally, sediment basins on construction sites have used riser structures as the primary mechanism for dewatering (Perez et al., 2018). These riser structures are usually constructed of aluminum pipe with holes drilled vertically and then wrapped in a geotextile and backfilled with aggregate to serve as a filtration method. If correctly designed, perforated riser structures have been reported to have an effective sediment capture of 88% or higher (Edwards et al., 1999; Fennessey & Jarrett, 1997; Ward et al., 1979). Conversely, poor design leads to accelerated dewatering and loss effective sediment capture (Millen et al., 1997). Accelerated dewatering in perforated riser structures occurs when the hydrostatic head increases in the basin water column. Rapid increases in hydrostatic head occurs following a storm event where significant amounts of sediment laden runoff enters the basin. Therefore, the perforated riser structure forestalls the ability of sediment to fall from suspension and results in higher sediment concentrations in the effluent. Figure 11 shows a perforated riser structure installed in an Alabama Department of Transportation (ALDOT) roadside sediment basin.

Figure 11 Riser Structure in ALDOT Sediment Basin (Perez, 2016)**.**

8.1.2 Floating Surface Skimmer

Surface skimmers are now common practice for dewatering of sediment basins and have been implemented as standard by several state Departments of Transportations (DOTs) and environmental agencies. Floating surface skimmers are floating devices that are attached by a drainage pipe which is attached to the basin's outlet. Studies have proven that skimmers are the most efficient form of basin dewatering because of their capability of dewatering from only the top of the water column (Zech et al., 2014). Dewatering from the top of the water column allows time for sediment particles to settle, draining the least turbid water from the top. The longer the dewatering time, the more sediment can settle. Studies have shown that most of the sediment loss in a basin with a skimmer installed occurs in the first five to nine hours after a storm (Millen et al., 1997; Vaughan and Jarrett, 2001). Thus, longer detention and dewatering times are more desirable. It is important for sediment basins to have long enough detention times to allow for proper

sedimentation and dewater at a proper rate to provide available storage for future storm events. When compared to perforated riser structures, surface skimmers are much easier to install and require less maintenance. Also, floating surface skimmers allow for higher amounts of sediment capture in a basin. Jarrett (2001) investigated sediment loss in basins using a perforated riser pipe and a floating surface skimmer as principal spillways. The study revealed that sediment loss was 1.8 times higher when using a perforated riser than when using a skimmer. Additionally, studies have proven that floating surface skimmers can provide 96.8% sediment capture (Millen et al., 1997). Additionally, most skimmer products have an adjustable orifice so properly size the skimmer to meet detention requirements which also gives skimmers an advantage over riser structures.

8.2 FAIRCLOTH SKIMMER®

This section aims to best describe the purpose and design of the Faircloth Skimmer®, one of the many different types of skimmers commercially available. The Faircloth Skimmer is regarded as the first product to dewater sediment basins from the surface and led to the development of several other types of skimmers.

There are a variety of skimmer manufacturers, designs, and sizes. The skimmer used for this study was a 6-in. (15.2 cm) post-construction Faircloth Skimmer®. This design is a prototype, and no drawings currently exist. Figure 12 shows a cut sheet for the traditional sediment basin Faircloth Skimmer ®. The style of this skimmer and basic components are very similar to the post-construction skimmer used for this research. The main difference is the inlet of the skimmers. The skimmer shown in Figure 12 has a 6-in. (15.2 cm) diameter orifice as an inlet while the skimmer used in this study utilizes a sluice to drain water. According to calculations made by Faircloth Skimmer®, the 6-in. sediment basin skimmer has a dewatering capacity of 51,840 ft^3/day, or 0.6

ft^3/s (1468 m^3/day or 0.017 m^3/s). The sluice on the post-construction skimmer allows for significantly higher flow rates because detention is not as an important factor in a post-construction permanent basin as available storage.

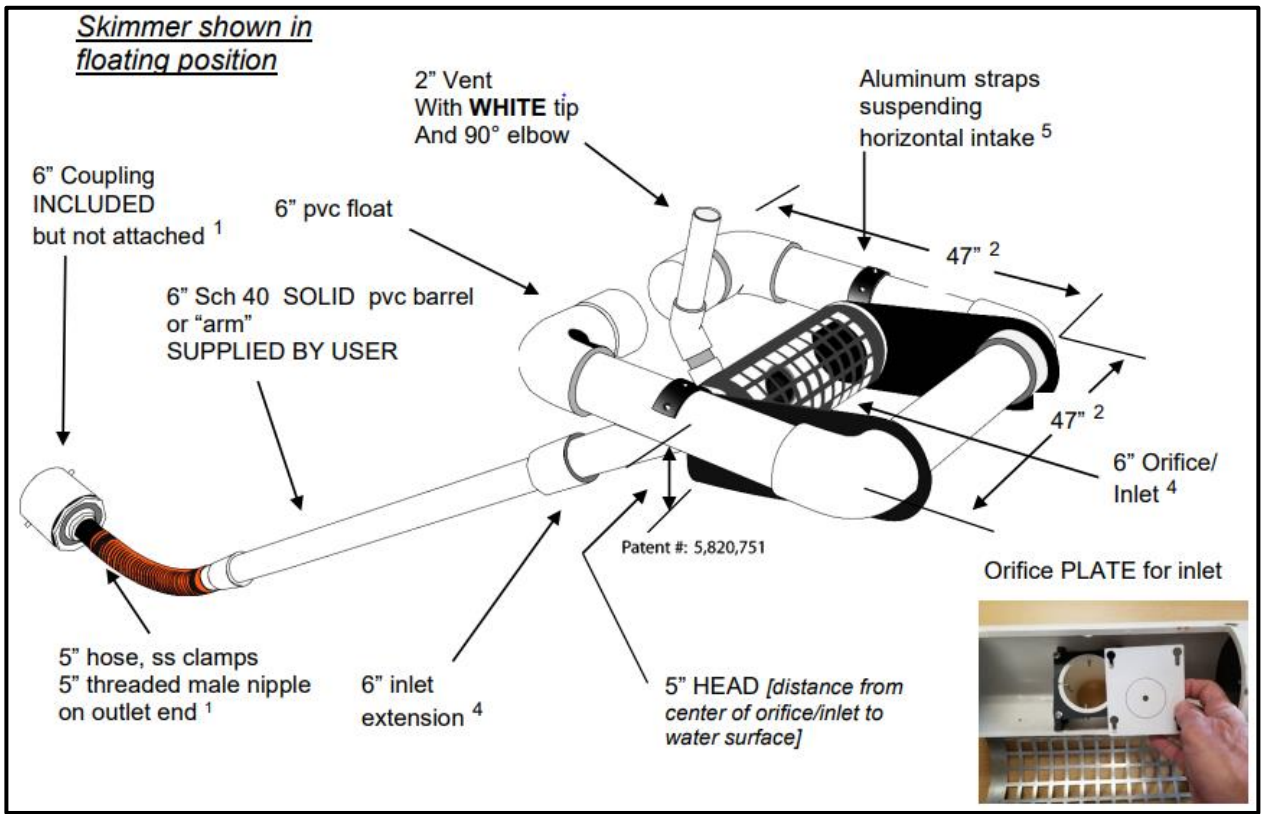

Figure 12 6 in. Faircloth Skimmer® Cut Sheet (J.W. Faircloth & Son, 2007) .

8.3 ASTM D8107 STANDARD TEST METHOD

The ASTM Standard D8107, entitled "*Standard Practice for Determining Sediment Pond Skimmer Flow Rate*" describes the procedures for experimental design and testing of a floating surface skimmer to determine clear water flow rate at various depths (ASTM D8107-18, 2018). This standard practice details guidelines, requirements, and procedures for large-scale, as installed, testing of a floating surface skimmer in a controlled experiment. It provides guidance for installation, execution, data collection, data analysis, and reporting results. For this study, ASTM

D8107 standards were followed with slight modifications to improve data collection and streamline the testing process.

The ASTM Standard D8107 testing apparatus consists of a calibrated basin with known surface area at any depth and is not less than 3.0 ft deep x 4.0 ft wide x 20.0 ft long (0.9 m deep x 1.2 m wide x 6.1 m long). The testing apparatus should also be fitted with a skimmer discharge pipe no smaller than the barrel joining the skimmer to the outlet. The tank shall have a valve at the outlet to stop or initiate dewatering. Other components required for the testing tank are a water delivery system and a depth measurement system mounted to the side of the tank to the nearest 0.039 in. (1.0 mm). Figure 13 shows a typical testing basin according to ASTM Standard D8107 in a study performed by Sprague et al., (2015).

Figure 13 ASTM D8107 Testing Basin (Sprague et al., 2015)**.**

Before testing begins, the tank discharge outlet and skimmer connections should be inspected to ensure a watertight seal. The valve on the discharge pipe should be closed prior to filling the tank with water. Once the tank is filled the water depth should be recorded using the ruler mounted on the side of the tank wall. Open the valve and allow the skimmer to dewater the tank while recording depth and time in at least 1-min. intervals. Skimmer flow rates are determined by the change in water depth over time, with known tank surface area. This process is to be triplicated for each evaluated skimmer. When reporting results, a plot of flow rate versus depth should be presented. Information such as testing facility, testing apparatus configuration, skimmer materials, testing procedures, data collection, and data analysis is also reported.

One limitation of this study is the fashion in which the data is collected. When testing a floating surface skimmer with high flow rates, recording water depth on a tape measure opens an opportunity for human error. Over several tests, this form of data collection could result in lower accuracy and reliability of the results. Also, the dataset would be considerably smaller, especially when only recording depth in 1-minute intervals. Furthermore, this test is limiting the evaluation to a 4-ft (1.2 m) depth, when skimmers can perform differently at deeper impoundments.

8.4 CASE STUDY

The following is a review of a study conducted by Sprague et al., (2015). This study was the basis for developing ASTM Standard D8107 outlined previously. The purpose of this study was to study floating surface skimmers in a full scale, controlled environment. The authors made a hypothesis that each skimmer product has its own unique design that affect hydraulic performance and that discharge rate is dependent on the product design. They claimed that accurate discharge rates of skimmer products can only be determined through full-scaled testing.

Four different skimmer products were tested in this study. Testing procedures, data collection, and data analysis followed ASTM D8107 standards. The findings indicate that skimmer performance varied based on product design. For example, one 3-in. (7.6 cm) skimmer had a 60% higher flow rate than a different 3-in. (7.6 cm) skimmer product. Typically, a skimmer is referred to in specifications by inlet size. In this case, if a sediment basin calls for a 3-in. (7.6 cm) skimmer the dewatering times would differ drastically between the two products tested in this study. Figure 14 shows two graphs comparing skimmer flow rates to water depth for each product design and size tested. This study proved that flow rates can differ significantly product to product and experimental testing is the only true way to determine accurate performance.

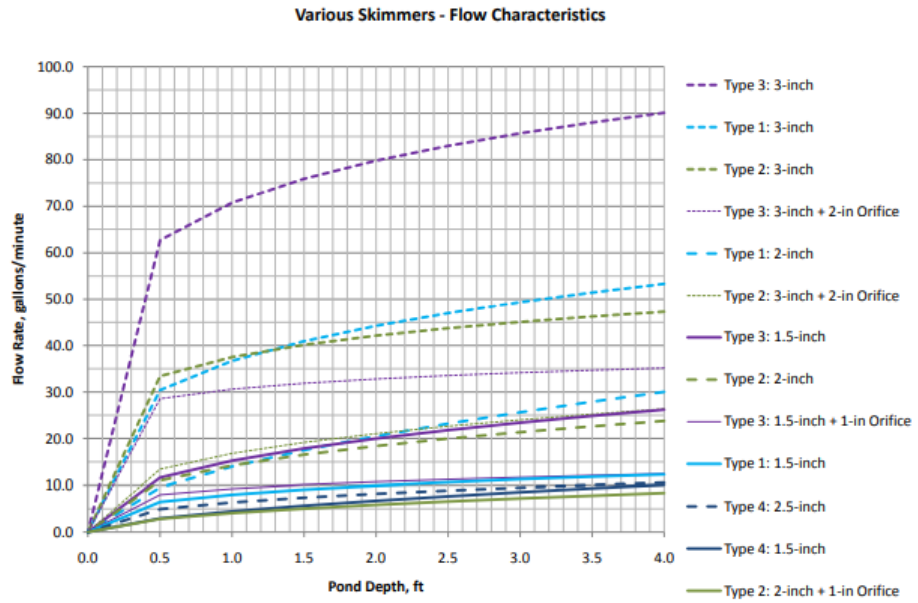

(a) Summary Graph 1; Flow Rate vs. Depth

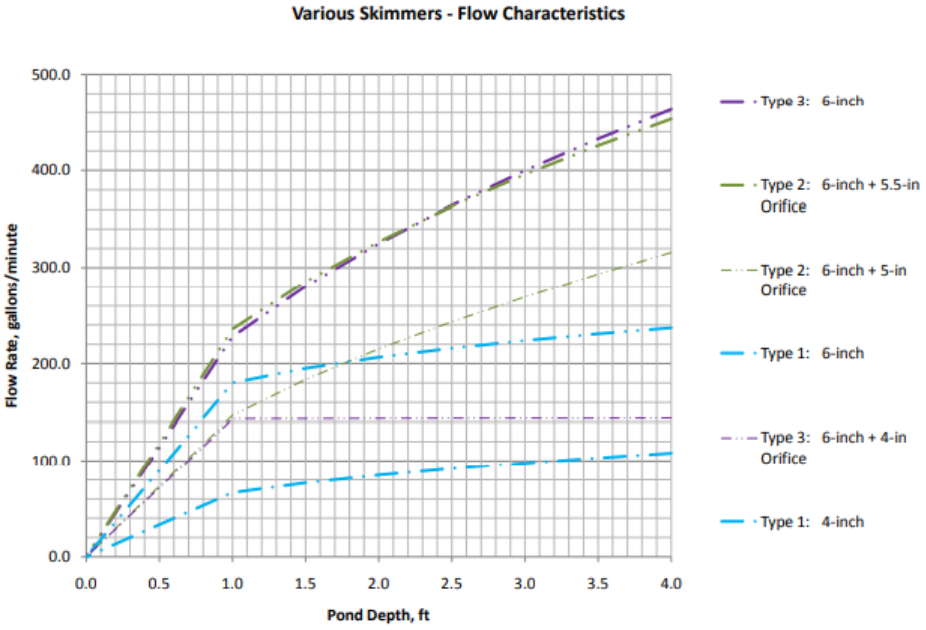

(b) Summary Graph 2; Flow Rate vs. Depth

Figure 14 Flow Rate vs. Water Depth Testing Results (Sprague et al., 2015)**.**

8.5 SKIMMER SELECTION AND SIZING

Correct sizing of a surface skimmer is important in sediment control design. Appropriate sizing is needed to achieve proper dewatering times. In a study conducted by Perez et al. (2018) a spreadsheet tool was developed to design basin geometry and volume, surface skimmer sizing, auxiliary spillway sizing, and baffle configuration. To determine surface skimmer sizing, the tool used equations to calculate required discharge rate. The calculations included parameters such as a discharge coefficient, orifice diameter, and head acting on the orifice. This discharge rate is used in Equation 8.1 below to determine the skimmer orifice size (Perez et al., 2018). The author states the dewatering calculation is a conservative approximation and the user should verify with the manufacturer to ensure the skimmer is correctly sized for the designed discharge.

$$O_{skim} = x * Q_{skim}^{2/5} \tag{8.1}$$

where,

O_{skim} = Skimmer Orifice Diameter (in or cm)

x = 2.8163 or 2.665, for SI or U.S. customary units, respectively

Q_{skim} = Required Discharge Rate (ft^3/s or m^3/s)

Faircloth Skimmer® has a method for determining skimmer size and the required orifice for its surface skimmers (Faircloth Skimmer® Surface Drain, 2007). The skimmer size is determined by the skimmer's maximum flow capacity based on typical drawdown requirements. The flow capacities are an approximation of the dewatering time at maximum capacity. The calculation tool used to determine skimmer size an orifice diameter states that the flow rates used in the calculation are theoretical values calculated by an equation using orifice size and water head on the inlet of

the skimmer. Figure 15 below shows the flow capacities listed for each skimmer to aid in skimmer sizing for a sediment basin.

1½" skimmer:	1,728 cubic feet in **24 hours**	6,912 cubic feet in **4 days**
with a 1½" head	3,456 cubic feet in **2 days**	12,096 cubic feet in **7 days**
	5,184 cubic feet in **3 days**	
2" skimmer:	3,283 cubic feet in **24 hours**	13,132 cubic feet in **4 days**
with a 2" head	6,566 cubic feet in **2 days**	22,982 cubic feet in **7 days**
	9,849 cubic feet in **3 days**	
2½" skimmer:	6,234 cubic feet in **24 hours**	24,936 cubic feet in **4 days**
with a 2.5" head	12,468 cubic feet in **2 days**	43,638 cubic feet in **7 days**
	18,702 cubic feet in **3 days**	
3" skimmer:	9,774 cubic feet in **24 hours**	39,096 cubic feet in **4 days**
with a 3" head	19,547 cubic feet in **2 days**	68,415 cubic feet in **7 days**
	29,322 cubic feet in **3 days**	
4" skimmer:	20,109 cubic feet in **24 hours**	80,436 cubic feet in **4 days**
with a 4" head	40,218 cubic feet in **2 days**	140,763 cubic feet in **7 days**
	60,327 cubic feet in **3 days**	
5" skimmer:	32,832 cubic feet in **24 hours**	131,328 cubic feet in **4 days**
with a 4" head	65,664 cubic feet in **2 days**	229,824 cubic feet in **7 days**
	98,496 cubic feet in **3 days**	
6" skimmer:	51,840 cubic feet in **24 hours**	207,360 cubic feet in **4 days**
with a 5" head	103,680 cubic feet in **2 days**	362,880 cubic feet in **7 days**
	155,520 cubic feet in **3 days**	
8" skimmer:	97,978 cubic feet in **24 hours**	391,912 cubic feet in **4 days**
with a 6" head	195,956 cubic feet in **2 days**	685,846 cubic feet in **7 days**
	293,934 cubic feet in **3 days**	

Figure 15 Faircloth Skimmer Sizing Sheet (*Faircloth Skimmer ® Surface Drain*, 2007).

The second step in this process is to calculate the orifice size to adjust the flow rate and customize the skimmer to the sediment basin's volume. This step is only required if the capacities listed above do not meet the desired drawdown time. The orifice size is calculated by using required area of the orifice. The required area is calculated by dividing the basin volume by a precalculated factor for each skimmer size and drawdown time required. Required area is then

used to determine the radius of orifice. The user can then adjust the opening size of the orifice based on the calculation. Once again, this method is a rough estimate of skimmer size selection and orifice opening. The values are theoretical and do not account for flow rate changing as depth of the water column changes.

CHAPTER NINE: MEANS AND METHODS

9.1 INTRODUCTION

The following section describes the procedures and methodology for experimental testing and evaluation of the skimmer. The methods developed for testing are based on standard practices with slight modifications for improvement. Testing methods and procedures, along with modifications, aim to provide performance evaluations of the skimmer and make improvements to current standard practices in testing. The goal of experimental testing was to evaluate the skimmer to provide an accurate assessment of flow rate performance through controlled testing.

9.2 EXPERIMENTAL DESIGN & PROCEDURE

9.2.1 Testing Location

Testing was conducted at the Auburn University Stormwater Research Facility (AU-SRF) in Opelika, AL. The 10-acre (4.0-hectare) outdoor research facility is used for conducting full-scale tests to evaluate and improve practices and products in stormwater management. The facility was developed in 2009 in collaboration with the Auburn University Highway Research Center and the Alabama DOT. The AU-SRF also serves as a location to train contractors and designers on proper practices. Of the various stormwater practices evaluated at the AU-SRF, surface skimmer dewatering flow rates can be tested in the skimmer evaluation tank (Figure 16).

Figure 16 Skimmer Evaluation Tank at AU-SRF.

9.2.2 Skimmer Evaluation Tank

The skimmer evaluation tank was originally installed at the AU-SRF by Dr. Michael Perez in 2015. The tank is made up of a modified 40 yd^3 (31 m^3) steel roll-off dumpster that was donated by Republic Services ®. Prior to site delivery, the tank was welded shut to make for a water-tight system. An 8 in. (20 cm) and a 4 in. (10 cm) flange were installed at the bottom of the tank to allow for skimmer connections and dewatering. A 4 ft (1.2 m) deep excavation was made, and the tank was placed and leveled. An 8 in. (20 cm) outlet pipe buried underground that allows the tank to discharge water into the adjacent retention pond. After installation and leveling, the excavation was backfilled and compacted. Initial trials revealed that leaking existed along weld locations. To prevent leaking, the tank was lined with polyurea, a material commonly found in truck beds, to ensure a water-tight seal. The tank (Figure 17) has length of 21.8 ft, width of 6.9 ft, and a height of 7.0 ft (6.64 m length, 2.1 m width, and 2.1 m height). This gives a bottom surface area of 150.42

ft^2 (13.974 m^2) and a volume of approximately 1,053 ft^3 29.82 m^3) when water level reaches the top of the tank (7.0 ft) (2.1 m). This information was important and essential to the testing procedure. The original "L" shaped skimmer fitting at the outlet was removed to create more room for the skimmer once installed.

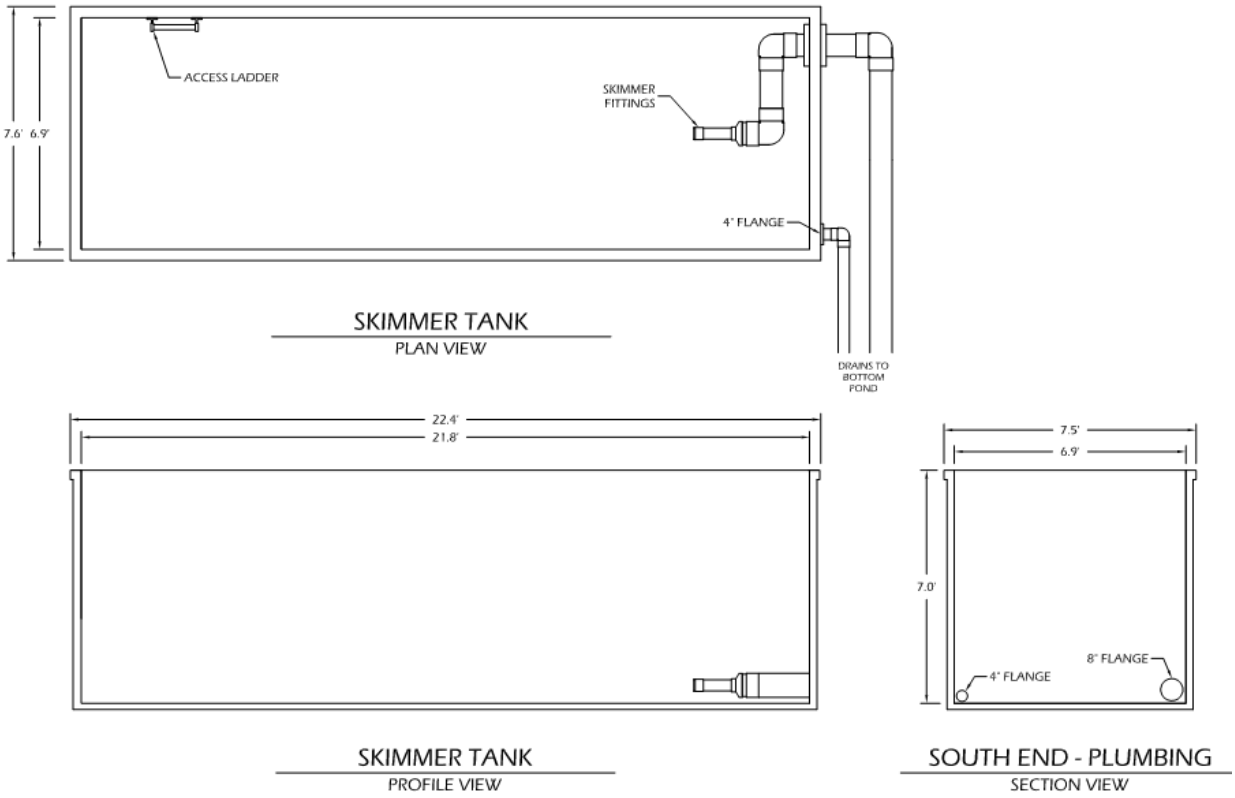

Figure 17 Skimmer Evaluation Tank at AU-SRF.

9.2.3 Water Delivery System

The tank was outfitted with a water delivery system constructed of PVC pipe connected to a series of DuroMax® XP904WP pumps with a capacity of 1.0 ft^3/s (0.028 m^3/s), and a 4 in. (10 cm) hose connection. Pumps were placed at the adjacent retention pond and 4 in. (10 cm) lay flat hoses connected umps to the PVC delivery system. Four PVC pipe delivery systems were constructed to fill the tank faster so that testing time could decrease, thus increasing the number of

experiments conducted. Figure 18 below illustrates the skimmer evaluation tank outfitted with four PVC delivery systems and connection locations for the pumps. The PVC pipe delivery systems were placed on the side wall of the tank in a "T" shape with water pumped out to the sides so that the buoyancy effects of incoming water on the skimmer would be minimized. When combined, the total water delivered to the tank was approximately 4.0 ft^3/s (0.11 m^3/s).

(a) Skimmer Evaluation Tank (Skimmer Installed)

(b) PVC Pipe Water Delivery System

(c) Adjacent Retention Pond

(d) Delivery System Connection

Figure 18 Skimmer Evaluation Tank and Water Delivery System.

9.2.4 Skimmer Apparatus

The skimmer used for experimental testing was a prototype provided by J.W. Faircloth & Son, Inc. This skimmer is intended to be used for post-construction stormwater management in a permanent retention pond. The skimmer is constructed with schedule 40 PVC pipe with a barrel and flexible hose to connect the skimmer to the tank outlet (Figure 19). Commonly, skimmers contain an orifice that is adjustable to control flow. For the skimmer provided for this research, the flow was controlled by an adjustable sluice gate which allowed water to run underneath. The sluice gate opening ranged from 0.5-in. to 6-in. (1.3 cm to 15 cm) and was adjustable in 0.5-in. (1.3 cm) intervals. A 6-in. (15 cm) schedule 40 PVC pipe, or barrel, connected the inlet of the skimmer to the flexible hose which connected to the tank outlet. The barrels provided for testing were an 8-ft (2.4 m) barrel and a 4-ft (1.2 m) extension to create a 12-ft (3.6 m) barrel. The 8-ft and 12-ft (2.4 m and 3.6 m) barrel lengths are typically the minimum and maximum lengths used in practice, respectively. The inlet of the skimmer was covered by a transparent plastic material so flow patterns could be observed during testing. Also, a ventilation pipe was inserted where the simmer connected to the barrel. This would allow different flow conditions to be tested.

(a) Faircloth Skimmer & Barrel

(b) Adjustable Sluice Gate

(c) Sluice Gate Adjustable Ports

(d) Flexible Hose Attachment

Figure 19 Skimmer Installation in Evaluation Tank.

9.3 DATA COLLECTION

The purpose of this research was to evaluate skimmer flow rates to provide an accurate assessment of performance. Two methods of data collection were used in initial testing. A Teledyne Isco® 2150 Area Velocity Flow Module and Sensor was installed at the outlet of the discharge pipe to the retention pond. The sensor was secured with a steel collar that fastens to the inside of the discharge pipe and the sensor was centered at the bottom of the pipe. The module was programmed to determine flow rate based on the area-velocity method which requires the height of water flow and pipe diameter as inputs.

The second form of data collection was by using a Solinst Levelogger® 5 Model 3001 and Solinst Barologger® 5 Model 3001. A Levelogger® is a data logger that collects and records fluctuations in water depth in specified time intervals. Using the Solinst® module, the logger can be programmed to the experimental setup. A Levelogger® measures water and atmospheric pressure; therefore, the Barologger® is used to compensate for atmospheric pressure. Data from both loggers can be downloaded in the Solinst Levelogger® Software where both data files are combined to adjust for atmospheric pressure (psi). This creates a file of water pressure measured in feet of water. For the skimmer testing procedure, the Levelogger® was secured inside a PVC pipe and zip-tied to the bottom an access ladder in the tank (Figure 20). The bottom offset from the bottom of the Levelogger® to the floor of the tank was 0.25 ft (0.076 m). This offset is programmed in the initial setup and is compensated for while determining total water depth. The final setting to be programmed is the time interval for data collection which was set to five seconds for the experiment. Water depths were multiplied by the surface area of the tank to determine the volume of water discharged every 5 seconds.

A tape measure was adhered to the side of the tank as a way of confirming the data being collected by the flow meter and Levelogger®. During testing, water level would be recorded on the tape and then timed in 1-ft (0.3 m) intervals. The flow rate determined by this method assured that the two other methods of data collection were reliable.

(a) Solinst Levelogger® secured at tank floor

(b) Tape measure adhered to tank wall

(c) Solinst Levelogger® 5 Model 3001
(Solinst, 2021)

(d) Isco® 2150 Area Velocity Flow Module and Sensor
(Isco, 2019)

Figure 20 Data Collection Measures for Skimmer Testing.

9.4 EXPERIMENTAL TESTING PROCEDURE

Once all components listed in the sections above were in place, skimmer testing would begin by setting the sluice gate opening size. A separate, detachable, gate was used to slide in front of the opening to prevent the skimmer from draining any water. This would decrease testing time and did not constrain testing to the capacity supplied by the pumps. Next, the four pumps were turned on and supplied water at a rate of approximately 4.0 ft^3/s (0.11 m^3/s). Pumps were ran until the water level reached the top of the tank. Once water reached the 83 in. (211 cm) mark the tank was considered full. This measure was taken to ensure repeatability of the testing procedure. When

the tank was full, the pumps were all cut off and the detachable was removed so the skimmer could begin to dewater the tank.

Once dewatering began, the Levelogger® and flow meter collected data in synchronized 5 second intervals. As the skimmer dewatered the tank, visual and audible observations were made of the skimmer to determine flow tendencies based on water depth. Once the skimmer drained the entire tank and rested on the tank floor, usually the 4 in. (10 cm) mark on the tape measure, the sluice gate was adjusted to the next opening size to be tested. The testing procedure was designed to be repeatable so results would be consistent. These tests were repeated so that the 1, 2, 3, 4, 5, and 6 in. (2, 5, 8, 10, 13, and 15 cm) sluice gate openings would have three tests each using an 8-ft and 12-ft (2 m and 4 m) barrel. This resulted in a total of 36 tests conducted on the skimmer.

9.5 DATA ANALYSIS

The goal of the initial data analysis was to determine the accuracy and validity of each data collection method. The most effective way of determining skimmer performance was to evaluate flow rate as a function of water depth. Water depth recordings from the Levelogger® were multiplied by the tank surface area (150.4 ft^2) (13.974 m^2) to obtain the volume of water in the tank. Flow rates were then determined by calculating the volume change in the tank in the 5 second time interval. Flow rate of the skimmer could then be plotted against water depth. The flow meter was recording flow rates in the same time intervals as the Levelogger®, so flow rate data from the flow meter were plotted against water depth. Finally, a comparison of the two data collection methods was made to determine the most accurate and precise method. Figure 21 presents results from a preliminary test showing data from both the Levelogger® and flow meter.

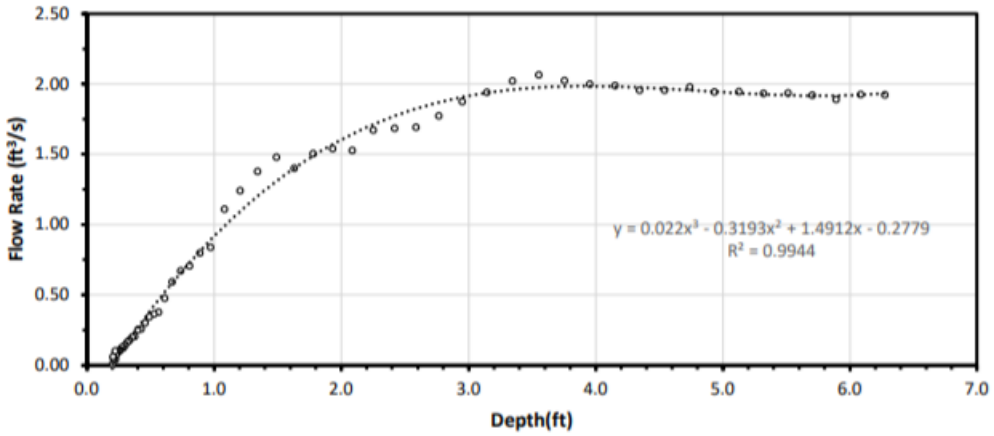

(a) Flow Rate vs. Depth for Levelogger®

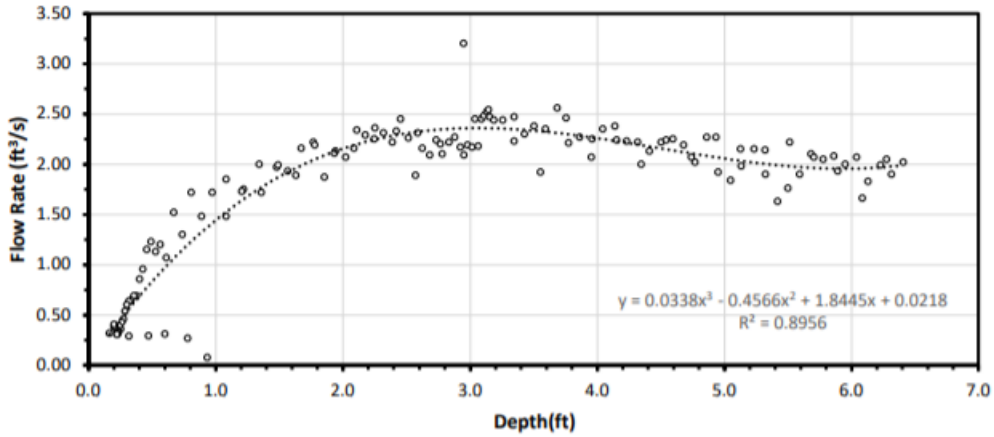

(b) Flow Rate vs. Depth for Flow Meter

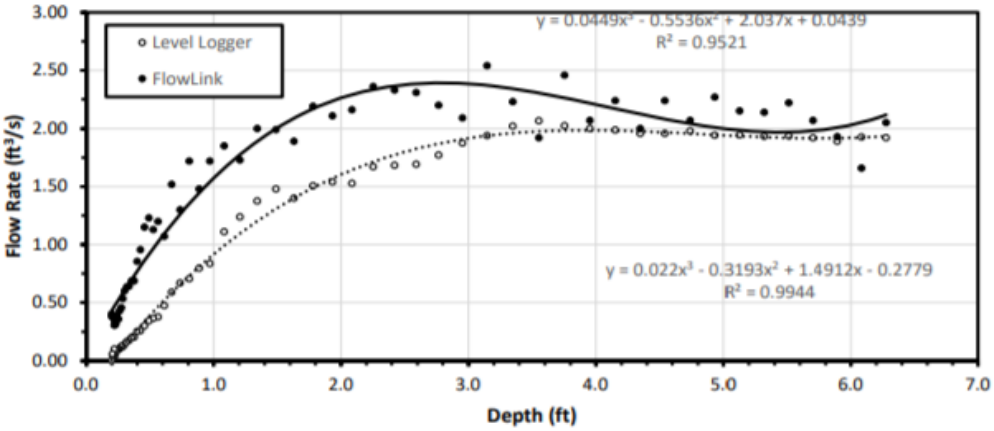

(c) Levelogger and Flow Meter vs. Depth

Figure 21 Initial Comparison of Data Collection Methods.

Upon comparison, it was determined that flow rate data from the Levelogger® was more consistent and reliable than that of the flow meter. The R^2 value for the Levelogger® best-fit line

was 0.9944 and 0.8956 for the flow meter, indicating the Levelogger® trendline more accurately represents the dataset. Also, flow rates from the Levelogger® were consistent with manual flow rate calculations visually recorded with the tape measure and stopwatch during testing. Furthermore, the flow meter yielded much higher results for flow rate. The reasoning behind the inconsistency of the flow meter is likely due to high flow rates and turbulence in the discharge. Any slight change in water level in the outlet pipe or water velocity would create variations in flow rate results when using the area velocity method. This problem was not experienced using the Levelogger® because the surface was placid and the decrease in water level was very steady as the skimmer dewatered the tank. Due to these reasons, the decision was made to abandon the flow meter and rely on results provided by the Levelogger®.

CHAPTER TEN: RESULTS AND DISCUSSION

10.1 EXPERIMENTAL RESULTS

After preliminary analyses were complete, data analysis was continued using data collected from the Levelogger®. plots for flow rate as a function of depth were created for each of the 36 tests completed. Figure 22 is a flow rate vs. depth graph for the 1.0 in. (2.5 cm) opening while using the 8.0 ft (2.4 m) barrel. This graph consists of data combined from the three tests completed with this skimmer configuration.

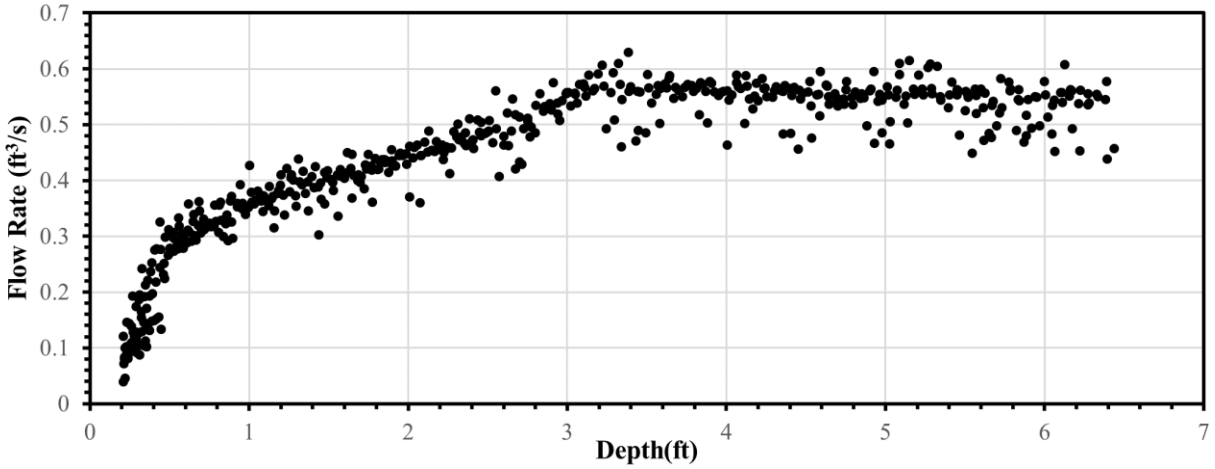

Figure 22 Flow Rate vs. Depth: 1 in. Opening; 8 ft Barrel.

Once flow rate graphs were created for all 36 tests, plots were examined to find trends in the data. The goal was to create a model so that the skimmer flow rate could be predicted at a given water depth under 7.0 ft (2.1 m). An observation was made that the graphs were all divided into 3 or 4 linear sections. For example, Figure 22 above has a linear section from 6.5 ft to approximately 3.0 ft (2.0 m to 0.91 m), from 3.0 ft (0.91 m) to approximately 0.5 ft (0.2 m), and from 0.5 ft (0.2 m) to 0 ft. This method was used to create the model to predict flow rate. Figure 23(a) is the same graph above with linear trendlines added with the line equations used to create the model. Figure

23(b) shows the final model for the 1-in. (1.3 cm) sluice gate opening and 8 ft (2.4 m) barrel configuration.

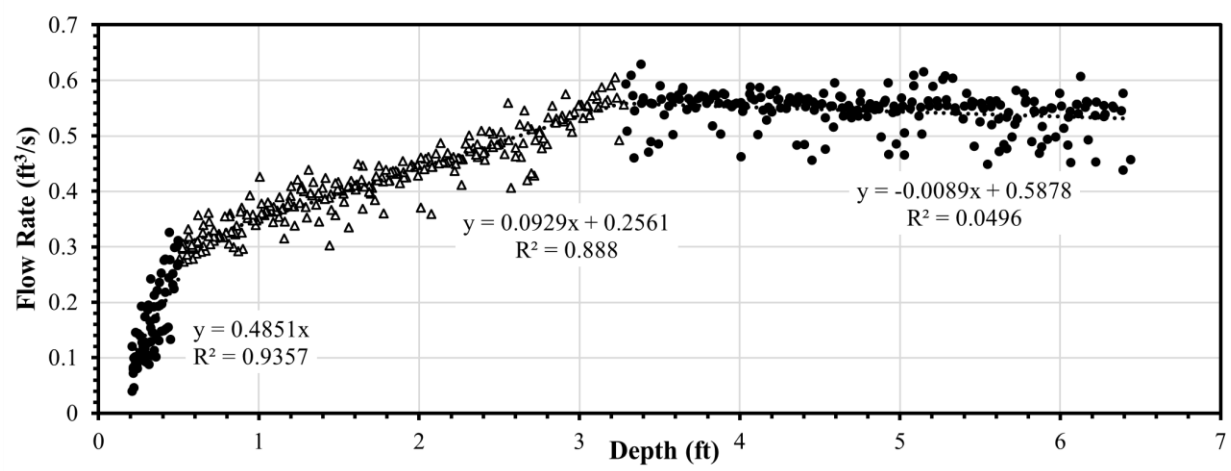

(a) Flow Rate vs. Depth with Linear Trendlines

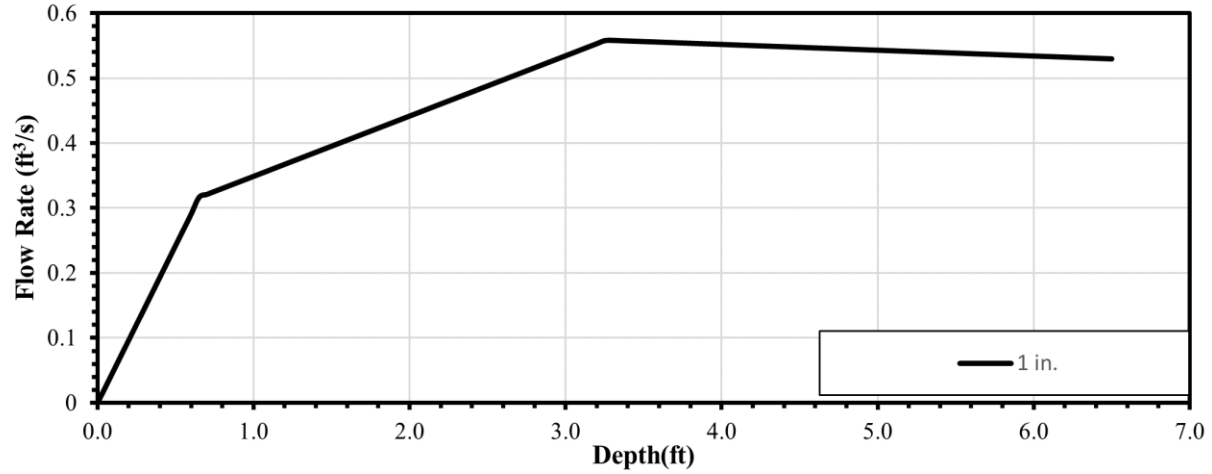

(b) Flow Rate vs. Depth Model

Figure 23 Flow Rate vs. Depth with Trendlines and Model: 1 in. Opening; 8 ft Barrel.

This data analysis process was performed for each of the 36 tests performed. Figure 24(a) and (b) below show the combined flow rate vs. depth data points for an 8 ft and 12 ft (2.4 m and 3.7 m) barrels. Figure 24(c) is a combined model for tests using both barrel lengths. Starting with a 1.0 in. (2.5 cm) opening, the maximum flow rate reaches approximately 0.5 ft^3/s (0.01 m^3/s). As the sluice gate opening size increases by 1.0 in. (2.5 cm), the maximum flow rate increases by

nearly 0.5 ft^3/s (0.01 m^3/s). The final opening size of 6.0 in. (15 cm) has a maximum flow rate upwards of 2.5 ft^3/s (0.07 m^3/s).

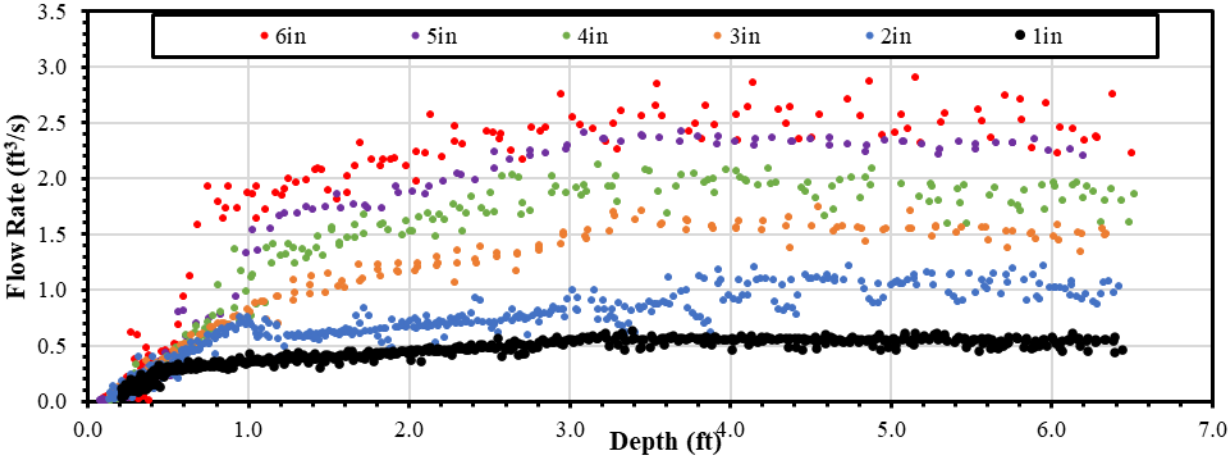

(a) 8 ft Barrel Dataset

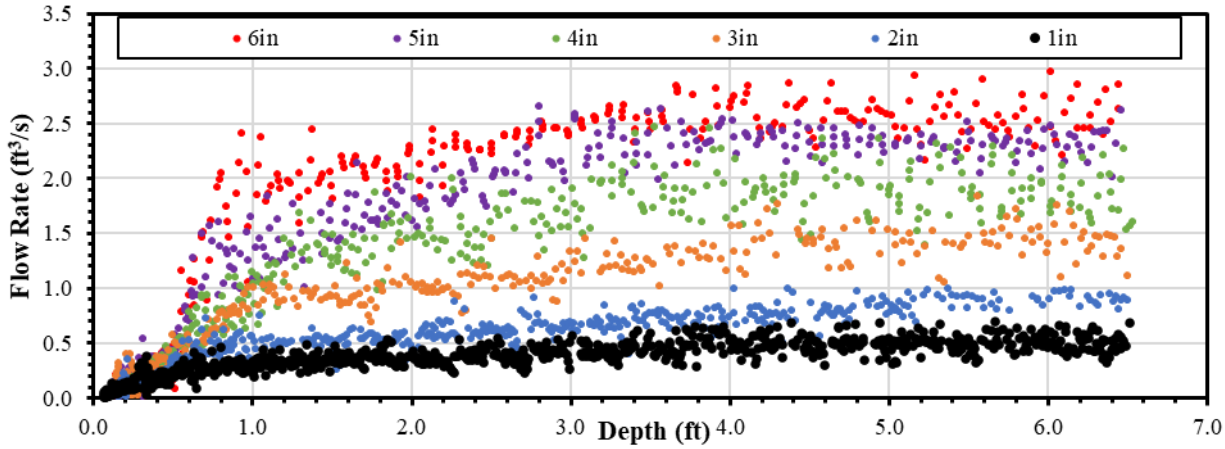

(b) 12 ft Barrel Dataset

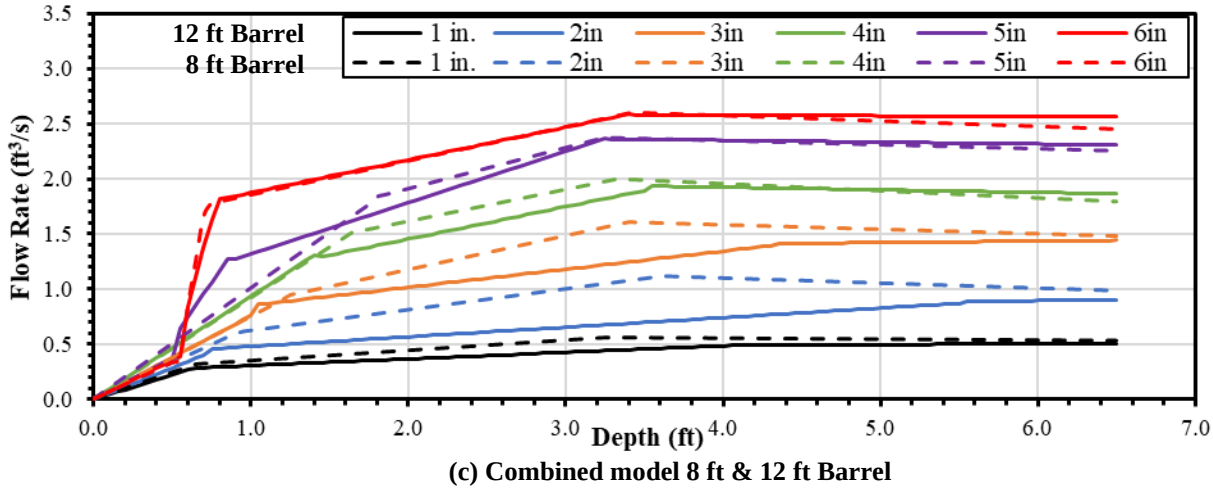

(c) Combined model 8 ft & 12 ft Barrel

Figure 24 Flow Rate vs. Depth Final Datasets and Models.

Figure 24 shows that the performances of both barrel lengths are similar, but not identical. For a 1.0-3.0 in. (2.5-7.6 cm) opening, the 8 ft (2.4 m) barrel has a more noticeable transition and continues to dewater at its maximum rate for a longer period than the 12 ft (3.7 m) barrel. This is likely due to the angle of the barrel in the tank at maximum depth. The increased angle of the shorter barrel would likely increase water velocity in the barrel. Additionally, the shorter barrel causes the skimmer to float lower in the water at higher depths. This increases the water head at the sluice inlet which increases flow rate. When the 12 ft (3.7 m) barrel is installed, the angle of the barrel will be decreased when at maximum depth and the water head at the inlet will be decreased. This is likely causing the higher flow rate values when using a shorter barrel length. Also, when using an 8 ft (2.4 m) barrel the flow rate appears to increase slightly as dewatering begins at maximum depth and continues until approximately 3.5 ft (1.1 m) in depth. The 12 ft (3.7 m) barrel is constant at maximum flow rate until nearly 3.5 ft (1.1 m). An audible observation was made that once the skimmer reached water depths where the abrupt changes in flow rate occur the sound of skimmer dewatering changed. This is because the barrel is either filled with water or has air flowing through. Based on these findings, it was determined that there is an optimal angle at which water will flow through the barrel at maximum velocity. It is recommended that further testing be conducted to determine how the angle of the barrel affects flow between both barrel lengths.

10.2 SKIMMER SIZING TOOL

After analyzing experimental results, it was determined that a tool would be made to predict flow rate based on the models. This would allow the results to be more easily implemented to aid design. The goal was to create a sizing tool that an engineer or designer would use to select the

appropriate skimmer opening size and barrel length combination based on the parameters of the basin.

Calculations for the sizing tool were based on the models created in the original data analysis. As stated previously, models were created by dividing flow rate vs. depth plots into 3 to 4 linear sections. The sections are independent to each opening size and barrel length configuration. Table 7 below is an example of the 1 in. (2.5 cm) opening and 12 ft (3.7 m) barrel configuration. This shows how the equations were divided into linear sections to create the model and how they were used to form the foundation of the sizing tool.

Table 7 Linear Equations to Create 1 in., 12 ft Barrel Model

Linear Equation	Parameters (ft)
$y= 0.4536(x)$	$0 \leq x \leq 0.6$
$y= 0.0600(x)+0.2465$	$0.6 < x \leq 4.0$
$y= 0.0067(x)+0.4631$	$x > 4.0$

The sizing tool was created using Microsoft Excel functions along with Visual Basics for Applications (VBA) coding. The combination of Excel functions and VBA code created an automated tool that provides the user with essential data for skimmer selection based on retention requirements. Factors such as flow rate, available storage, and design drawdown time are important for sizing and are determined by user input in the tool. Figure 25 represents an example of the sizing tool being used to determine drawdown time of an existing retention pond. User inputs and selection criteria are highlighted grey and design drawdown time is highlighted in blue.

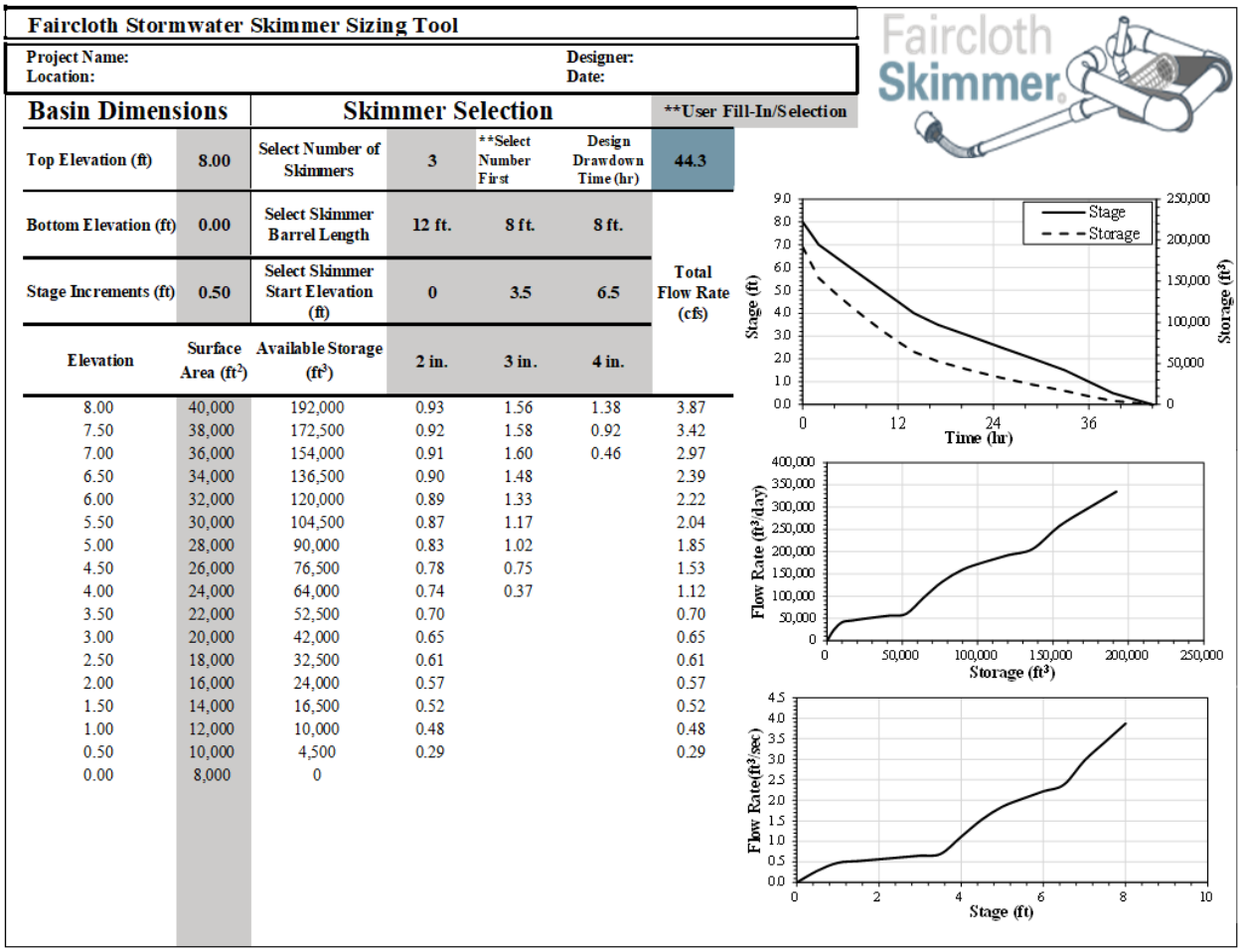

Faircloth Stormwater Skimmer Sizing Tool

Project Name: Location: Designer: Date:

Faircloth Skimmer®

Basin Dimensions		Skimmer Selection				**User Fill-In/Selection
Top Elevation (ft)	8.00	Select Number of Skimmers	3	**Select Number First	Design Drawdown Time (hr)	44.3
Bottom Elevation (ft)	0.00	Select Skimmer Barrel Length	12 ft.	8 ft.	8 ft.	
Stage Increments (ft)	0.50	Select Skimmer Start Elevation (ft)	0	3.5	6.5	Total Flow Rate (cfs)

Elevation	Surface Area (ft^2)	Available Storage (ft^3)	2 in.	3 in.	4 in.	
8.00	40,000	192,000	0.93	1.56	1.38	3.87
7.50	38,000	172,500	0.92	1.58	0.92	3.42
7.00	36,000	154,000	0.91	1.60	0.46	2.97
6.50	34,000	136,500	0.90	1.48		2.39
6.00	32,000	120,000	0.89	1.33		2.22
5.50	30,000	104,500	0.87	1.17		2.04
5.00	28,000	90,000	0.83	1.02		1.85
4.50	26,000	76,500	0.78	0.75		1.53
4.00	24,000	64,000	0.74	0.37		1.12
3.50	22,000	52,500	0.70			0.70
3.00	20,000	42,000	0.65			0.65
2.50	18,000	32,500	0.61			0.61
2.00	16,000	24,000	0.57			0.57
1.50	14,000	16,500	0.52			0.52
1.00	12,000	10,000	0.48			0.48
0.50	10,000	4,500	0.29			0.29
0.00	8,000	0				

Figure 25 Stormwater Skimmer Sizing Tool Sheet.

To start, the user must input and select data criteria. The basin dimensions that must be entered are top elevation, bottom elevation, stage increment, and surface area at each elevation. These are dimensions that are typically found in the basin drawings. Once entered, the VBA code calculates and auto populates the elevation and available storage columns. If any change is made to a cell highlighted in grey the code is activated and the cells are repopulated. Available storage is calculated using the average end area method (Equation 10.1). Incremental storage is calculated and accumulated for each cross section to determine the available storge at each elevation.

$$V = \frac{A1 + A2}{2} * h \quad (10.1)$$

where,

V = Incremental Volume (ft^3)

$A1$ = Area of Upper Cross Section (ft^2)

$A2$ = Area of Lower Cross Section (ft^2)

h = Elevation Difference in Cross Sections (ft)

Next, the user must select skimmer criteria from drop down lists highlighted in grey. The user may select 1 to 3 skimmers to be used for the basin. In large post-construction stormwater basins, multiple skimmers can be used in unison or in stages to dewater the basin. Allowing the user to select multiple skimmers gives the option to design for this scenario. In the example configuration above, the user would be selecting 3 skimmers to dewater the basin. After selecting number of skimmers, the user selects either an 8 or 12 ft (2.4 or 3.7 m) barrel for each skimmer and selects opening size for the sluice gate, ranging from 1.0 to 6.0 inches (2.5 to 15 cm). Opening size and barrel length selections are programmed into the Excel functions to select correlated flow rates. The final selection that must be made is start elevation of the skimmer. This option was created in the event of multiple skimmers being used in a staggered configuration. In this case the skimmer barrels connect to the outlet riser pipe in increasing height. With this configuration the skimmer is placed on a platform or stand and does not begin to dewater the basin until water level reaches the skimmer. Staggered configurations allow more control of dewatering rates of the basin. Figure 26 is an illustration of a project in New Zealand that placed three skimmers in a staggered fashion to dewater the basin.

Figure 26 Staggered Skimmer Configuration on New Zealand Project.

Once all user criteria have been entered or selected, all data in white cells is auto populated. The final column is total flow rate which takes the sum of each skimmer in use at that elevation. Total flow rate is used to calculate design drawdown time. Drawdown time is calculated by dividing basin storage by total flow rate. Table 8 shows how calculations for design drawdown time were made for the tool in the example used.

Table 8 Incremental and Cumulative drawdown time Calculations

Elevation (ft)	Total Flow Rate (ft^3/s)[a]	Inc. Drawdown (hr)	Cum. Drawdown (hr)
8	3.9	1.40[b]	0.00
7.5	3.4	1.50	1.40
7	3.0	1.63	2.90
6.5	2.4	1.92	4.53
6	2.2	1.94	6.46
5.5	2.0	1.97	8.39
5	1.8	2.03	10.36
4.5	1.5	2.26	12.39
4	1.1	2.86	14.66
3.5	0.7	4.18	17.52
3	0.7	4.03	21.70
2.5	0.6	3.86	25.73
2	0.6	3.67	29.60
1.5	0.5	3.44	33.27
1	0.5	3.18	36.71
0.5	0.3	4.38	39.89
0	0	0	44.26
		Total Drawdown (hr)	**44.26**

Notes: [a] Flow rate capacity for combined skimmers active at elevation
[b] Drawdown time from current to lower elevation

The user is also supplied with three graphs that are automatically filled for each change made to a cell highlighted grey. The three graphs created are stage and storage vs. time, flow rate vs. storage, and flow rate vs. stage (Figure 27). This gives the user a comprehensive summary of the results. The user can then adjust skimmer selection criteria such as number of skimmers, barrel length, start elevation, and opening size until the required drawdown times for the basin are met.

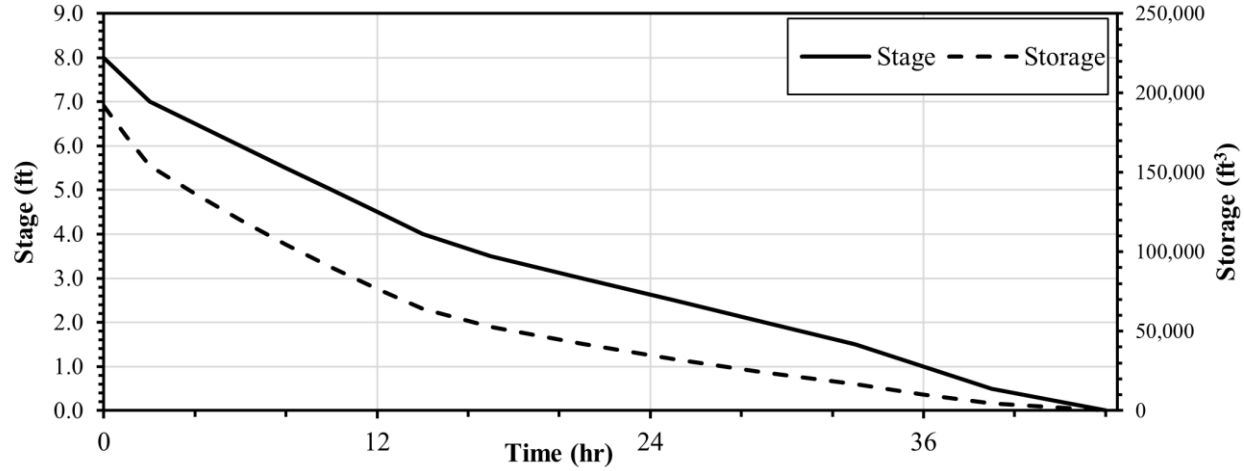

(a) Stage and Storage vs. Dewatering Time

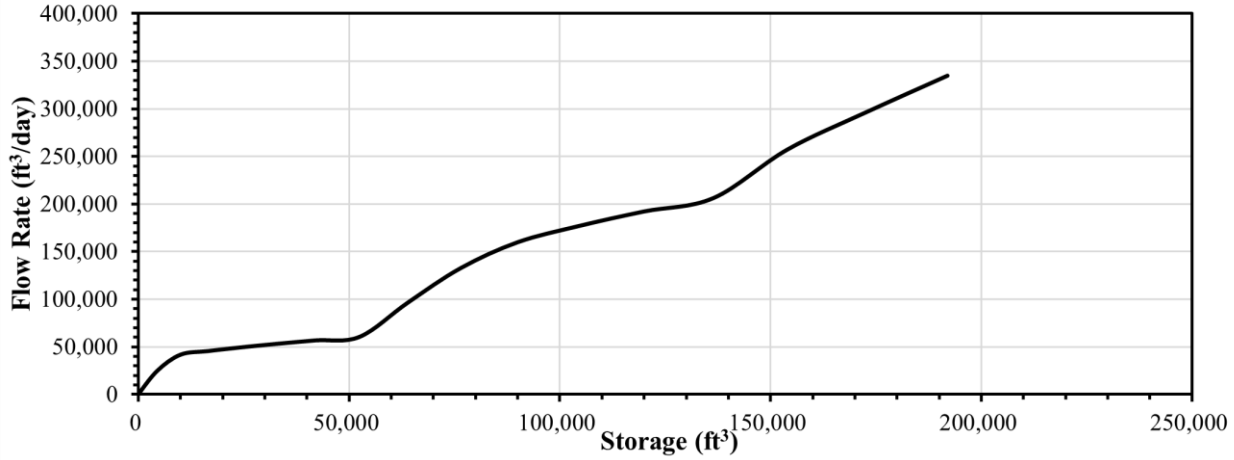

(b) Flow Rate vs. Basin Storage

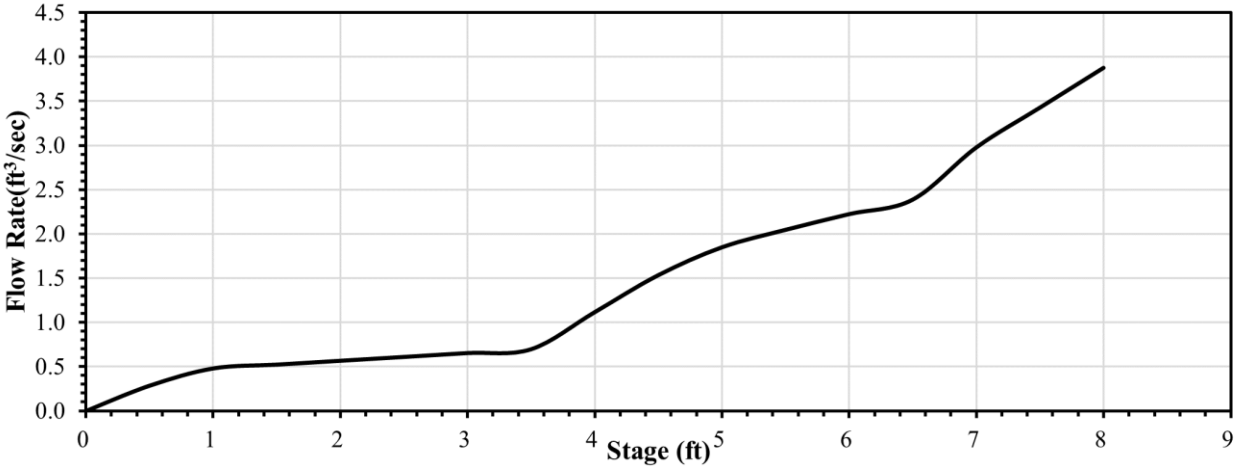

(c) Flow Rate vs. Basin Stage

Figure 27 Graphs from Skimmer Sizing Tool Example.

10.3 SUMMARY

This chapter provided results for testing flow rates of a post-construction stormwater skimmer in a controlled experiment. Experimental testing will provide designers and manufacturers with practical results of performance of this specific product. The methods of experimental design, data collection, and data analysis will be used, and improved upon, in future testing to further evaluate skimmer flow rate performance. Additionally, the Skimmer Sizing Tool can not only be used for sizing of the skimmer tested in this research, but easily expanded with future testing on other skimmer products.

CHAPTER ELEVEN: CONCLUSIONS AND RECOMMENDATIONS

11.1 CONCLUSIONS

Proper selection of erosion and sediment control practices and products is necessary to best manage stormwater on a construction site. Sediment basins are used to collect and treat stormwater runoff before leaving the construction site. As sediment laden water enters a basin, the sedimentation process begins through particle settling. Reaching an optimal balance between sedimentation and dewatering times is important to increase the efficiency of the sediment basin. Dewatering by way of a floating surface skimmer is the most effective way of discharging treated water from the sediment basin. Accurate dewatering rates are needed to properly for skimmer selection and sizing to meet detention requirements. Determining skimmer flow rates through experimental testing provides the most accurate data for selection and sizing. Previous studies prove significant variability in skimmer flow rates from product to product. Thus, experimental testing of skimmer flow rates is necessary to ensure reliable results.

The main contribution made through this study is proving that experimental testing is the most reliable method of determining skimmer flow rates at various heights. This study utilized a post-construction stormwater skimmer provided by J.W. Faircloth & Son, Inc. The two main objectives of the research were to determine skimmer flow rates at various water depths and to develop a skimmer selection and sizing tool with experimental data. ASTM D8107 standards were followed with slight deviations to improve data collection and streamline testing. Testing was performed in the skimmer evaluation tank at the AU-SRF in Opelika, AL. The evaluation tank allowed the skimmer to be tested at water depths up to 7 ft (2 m). A Solinst Levelogger® was the main source of data collection, recording water depth in the tank in 5-second intervals. Change in

water depth over the 5-second interval and the known surface area of the evaluation tank were used to determine flow rates at various heights for the post-construction stormwater skimmer. Three tests each were conducted for the 1, 2, 3, 4, 5, and 6-in. (2, 5, 8, 10, 13, and 15 cm) sluice gate opening sizes to create a sizable database for the creation of the skimmer sizing tool.

The skimmer sizing tool was created in Microsoft Excel and was intended to be interactive with the user and provide results to achieve the best skimmer configuration based on basin design and detention requirements. The sizing tool is intended for an engineer or designer who has access to specifications or drawings of the sediment basin as user input requires basin dimensions such as top and bottom elevation and surface area at the selected stage increments. For skimmer selection, the user is required to select the number of skimmers installed, barrel length, start elevation for dewatering, and gate opening size. Once basin and skimmer criteria are selected and entered the user is provided with data and graphs on flow rates, dewatering times, water depth, and basin storage. The user can then change skimmer criteria and determine the configuration to achieve the best balance of dewatering and available storage to meet detention requirements. The sizing tool is not exclusive to just the skimmer evaluated in this study but can be expanded with future testing of other skimmer products.

11.2 RECOMMENDED FURTHER RESEARCH

It is recommended that further research be conducted on various skimmer types and sizes using the skimmer evaluation tank at the AU-SRF. Since the skimmer evaluation tank is fitted with an 8-in. (20 cm) discharge outlet, any skimmer 8 in. (20 cm) or smaller can be easily installed for testing with the appropriate fitting. Testing different products and sizes will allow further comparisons of skimmer flow rates to be made.

Existing test procedures should remain with additional features added to increase knowledge of skimmer hydraulic properties. It is recommended that Leveloggers® be fastened to the base of the barrel, nearest to the discharge outlet, and at the barrel connection with the skimmer. With the two loggers in this configuration, the difference in elevation between the two could be recorded. Elevation difference could then be used to determine the angle of the barrel during testing. In this study it was revealed that higher flow rates occurred when the 8 ft (2.4 m) barrel was installed, opposed to the 12 ft (3.7 m) barrel. This rise in flow rate is more than likely due to the increased angle of the shorter barrel, increasing velocity of water in the barrel. Through this data collection method barrel angle could be compared with flow rate to determine the angle and which the maximum flow rate is experienced. This could be compared across numerous products and configurations to provide further insight into hydraulic characteristics of skimmers. Increased knowledge will facilitate proper selection and sizing of skimmers and increase efficiency of sediment basins.

The current skimmer sizing tool is only useful for the 6 in. (15 cm) post-construction skimmer used in this study. With further testing of different skimmer products, the skimmer sizing tool can be expanded. Flow rate data for different skimmers can be added to the tool and the user could have a wide range of selection criteria including manufacturer, product, inlet size, and barrel length to determine the best option for the sediment basin. Also, future studies on the reliability of the skimmer sizing tool should be conducted through field monitoring. This would allow the accuracy of the data and results provided by the tool to be field approved.

Finally, full scale testing under field conditions could be performed to evaluate skimmer flow rates along with sediment removal of stormwater entering the basin. Tests could determine how treatment of stormwater is affected by flow rate and decrease sediment in the effluent.

11.3 ACKNOWLEDGEMENTS

Part Two of this thesis is based on a study sponsored by J.W. Faircloth & Son, Inc. The author is grateful for the support. The findings, opinions, and conclusions conveyed in this thesis are those of the author and do not necessarily reflect the view of the sponsor.

REFERENCES

1. Akbari, H., Menon, S., & Rosenfeld, A (2009). “Global Cooling: Increasing World-Wide Urban Albedos to Offset CO2.” *Climatic Change*, 94(3–4), 275–286.
2. Alabama Department of Transportation (2020). “Standard Best Management Practices.” Montgomery, AL.
3. Alabama Soil and Water Conservation Committee (2018). "Alabama Handbook for Erosion Control, Sediment Control and Stormwater Management on Construction Sites and Urban Areas."Montgomery, AL.
4. ASTM C1371 (2015). “Standard Test Method for Determination of Emittance of Materials Near Room Temperature Using Portable Emissometers.” ASTM International, West Conshohocken, PA.
5. ASTM D8107 (2018). “Standard Practice for Determining Sediment Pond Skimmer Flow Rate.” ASTM International, West Conshohocken, PA.
6. ASTM E1918 (2021). “Standard Test Method for Measuring Solar Reflectance of Horizontal and Low-Sloped Surfaces in the Field.” ASTM International, West Conshohocken, PA.
7. ASTM E1980 (2011). “Standard Practice for Calculating Solar Reflectance Index of Horizontal and Low-Sloped Opaque Surfaces.” ASTM International, West Conshohocken, PA.
8. Berkeley Lab (2022). “Heat Island Group.” https://heatisland.lbl.gov/coolscience/cool-roofs
9. Cool Roof Rating Council (2019). “US Green Building Council’s Leadership in Energy and Environmental Design (LEED).” https://www.coolroofs.org/resources/leed

10. De Bin, R., Janitza, S., Sauerbrei, W., & Boulesteix, A. L. (2016). “Subsampling Versus Bootstrapping in Resampling-Based Model Selection for Multivariable Regression.” *Biometrics*, 72(1), 272–280.
11. Dixon, P. M. (2002). “Bootstrap Resampling.” *Encyclopedia of Environmetrics*. John Wiley & Sons, Ltd.
12. Dupuis, M. (2014). Quantitative Heat Transfer for Low-Slope Roof Membranes. *Symposium on Building Envelope Technology.* 23-33.
13. Edwards, C. L., Shannon, R. D., & Jarrett, A. R. (1999). “Sedimentation Basin Retention Efficiencies for Sediment, Nitrogen, and Phosphorus from Simulated Agricultural Runoff.” *Transactions of the American Society of Agricultural Engineers*, 42(2), 403–409.
14. Faircloth, J. W. (2007). “6" Faircloth Skimmer® Cut Sheet.” www.FairclothSkimmer.com
15. Faircloth, J.W. (2007). “Determining the Skimmer Size and the Required Orifice for the Faircloth Skimmer® Surface Drain.” www.FairclothSkimmer.com
16. Fang, X., Zech, W. C., & Logan, C. P. (2015). “Stormwater Field Evaluation and it’s Challenges of a Sediment Basin with Skimmer and Baffles at a Highway Construction Site.” *Water Environment Research*, 7(7), 3407–3430.
17. Fennessey, L. A. J., & Jarrett, A. R. (1997).“Influence of Principal Spillway Geometry and Permanent Pool Depth on Sediment Retention of Sedimentation Basins.” *Transactions of the American Society of Agricultural Engineers*, 40(1), 53–59.

18. Gentle, A. R., Aguilar, J. L. C., & Smith, G. B. (2011). “Optimized cool roofs: Integrating albedo and thermal emittance with R-value.” *Solar Energy Materials and Solar Cells*, 95(12), 3207–3215.
19. Grant, E. J., Black, K. A., & Werre, S. R. (2017). “The Influence of Roof Reflectivity on Adjacent Air and Surface Temperatures.” *Architectural Science Review*, 60(2), 137–144.
20. Green, A., Ledo Gomis, L., Paolini, R., Haddad, S., Kokogiannakis, G., Cooper, P., Ma, Z., Kosasih, B., & Santamouris, M. (2020). “Above-Roof Air Temperature Effects on HVAC and Cool Roof Performance: Experiments and Development of a Predictive Model.” *Energy and Buildings*, 222.
21. Hopfe, C. J., & Hensen, J. L. M. (2011). “Uncertainty Analysis in Building Performance Simulation for Design Support.” *Energy and Buildings*, 43(10), 2798–2805.
22. Ibrahim, S. (2009). “Sustainable Roof Design: More Than a Black-And-White Issue.” *Symposium on Building Envelope Technology.* 111-120.
23. Ibrahim, S. (2013). “The Un-Cool Consequences of Cool Roofing Cool Roof Systems are Not a Universal Fix for Climate Change and Energy Savings.” *Professional Roofing Magazine.* 1-4.
24. Ibrahim, S. (2013). “Where Does the Heat Go? A Look into Energy Performance of Reflective Membranes.” *RCI International Convention and Trade Show.* 71-78.
25. Iglewicz, B., & Hoaglin D. C. (1993). “How to Detect and Handle Outliers.” *American Society for Quality Control Statistics Division,* 16.
26. Jarrett, A. R. (2001). “Designing Sedimentation Basins for Better Sediment Capture.” *Soil Erosion*, 63–66.

27. Jo, J. H., Carlson, J. D., Golden, J. S., & Bryan, H. (2010). “An Integrated Empirical and Modeling Methodology for Analyzing Solar Reflective Roof Technologies on Commercial Buildings.” *Building and Environment*, 45(2), 453–460.
28. Lawrence, A. I., Marsalek, J., Ellis, J. B., & Urbonas, B. (1996). “Stormwater Detention & BMPs.” *Journal of Hydraulic Research*, 34(6), 799–813.
29. Levinson, R., & Akbari, H. (2010). “Potential Benefits of Cool Roofs n Commercial Buildings: Conserving Energy, Saving Money, and Reducing Emission of Greenhouse Gases and Air Pollutants.” *Energy Efficiency*, 3(1), 53–109.
30. Li, X. X., & Norford, L. K. (2016). “Evaluation of cool roof and vegetations in mitigating urban heat island in a tropical city, Singapore.” *Urban Climate*, 16, 59–74.
31. Mastrapostoli, E., Karlessi, T., Pantazaras, A., Kolokotsa, D., Gobakis, K., & Santamouris, M. (2014). “On the Cooling Potential of Cool Roofs in Cold Climates: Use of Cool Fluorocarbon Coatings to Enhance the Optical Properties and the Energy Performance of Industrial Buildings.” *Energy and Buildings*, 69, 417–425.
32. Millen, J. A., Jarrett, A. R., & Faircloth, J. W. (1997). "Experimental Evaluation of Sedimentation Basin Performance for Alternative Dewatering Systems.” *American Society of Agricultural Engineers*, 40(4), 1087–1095.
33. Oleson, K. W., Bonan, G. B., & Feddema, J. (2010). “Effects of White Roofs on Urban Temperature in a Global Climate Model.” *Geophysical Research Letters*, 37(3).
34. Osouli, A., Grinter, M., Zhou, J., Ahiablame, L., & Stark, T. (2017). “Effective Post-Construction Best Management Practices (Bmps) to Infiltrate and Retain Stormwater Run-Off.” *A report of the findings of ICT PROJECT R27-141 Effective Post-Construction*

Best Management Practices (BMPs) to Infiltrate and Retain Stormwater Run-Off. Illinois Center for Transportation.

35. Pakalapati, K. C. (2018). "Data Usage Optimization for Cost Estimating in Asphalt Paving Projects Using a Cost Indexing System." Master's Thesis, Auburn University.
36. Perez, M. A. (2014). "Evaluation of Inlet Protection Practices (IPPs) Using Large-Scale Testing Techniques." Master's Thesis, Auburn University.
37. Perez, M. A. (2016). "Improvements in the Design and Application of Erosion and Sediment Control Technologies for the Construction Industry." Doctoral Dissertation, Auburn University.
38. Perez, M. A., Zech, W. C., Donald, W. N., & Fang, X. (2016). "SEDspread: Sediment-Basin Design Tool for Construction Sites." *Journal of Irrigation and Drainage Engineering*, 142(12).
39. Perez, M. A., Zech, W. C., Fang, X., & Vasconcelos, J. G. (2016). "Methodology and Development of a Large-Scale Sediment Basin for Performance Testing." *Journal of Irrigation and Drainage Engineering*, 142(10).
40. Pisello, A. L., Santamouris, M., & Cotana, F. (2013). "Active Cool Roof Effect: Impact of Cool Roofs on Cooling System Efficiency." *Advances in Building Energy Research*, 7(2), 209–221.
41. Pitt, R., Clark, S., and Lake, D. W. (2007). "Construction Site Erosion and Sediment Controls: Planning, Design, and Performance." *DEStech Publications*, Lancaster, PA.
42. Roman, K. K., O'Brien, T., Alvey, J. B., & Woo, O. J. (2016). "Simulating the effects of cool roof and PCM (phase change materials) based roof to mitigate UHI (urban heat island) in prominent US cities." *Energy*, 96, 103–117.

43. Romeo, C., & Zinzi, M. (2013). “Impact of a Cool Roof Application on the Energy and Comfort Performance in an Existing Non-Residential Building. A Sicilian Case Study.” *Energy and Buildings*, 67, 647–657.
44. Schumacher, M. (1992). “A BOOTSTRAP RESAMPLING PROCEDURE FOR MODEL BUILDING: APPLICATION TO THE COX REGRESSION MODEL.” *STATISTICS IN MEDICINE*, 11, 2093-2109.
45. Seifhashem, M., Capra, B. R., Milller, W., & Bell, J. (2018). “The Potential for Cool Roofs to Improve the Energy Efficiency of Single Storey Warehouse-Type Retail Buildings in Australia: A Simulation Case Study.” *Energy and Buildings*, 158, 1393–1403.
46. Seo, S. (2006). “A Review and Comparison of Methods for Detecting Outliers in Univariate Data Sets.” Master’s Thesis, University of Pittsburg.
47. Solinst (2022). “Solinst 3001 Levelogger® 5: Water Level Datalogger.” https://www.solinst.com/products/dataloggers-and-telemetry/3001-levelogger-series/levelogger/. (March 4, 2022).
48. Sprague, J. E., Joel Sprague, C., & Ruzowicz, B. (2015). “EVALUATING FLOATING SURFACE SKIMMERS.” *2015 IECA Annual Conference.* Portland, OR.
49. Synnefa, A., Saliari, M., & Santamouris, M. (2012). “Experimental and Numerical Assessment of the Impact of Increased Roof Reflectance on a School Building in Athens.” *Energy and Buildings*, 55, 7–15.
50. Teledyne Isco (2019). “2150 Area Velocity Flow Module and Sensor Installation and Operation Guide.”

51. Testa, J., and Krarti, M. (2017). “A Review of Benefits and Limitations of Static and Switchable Cool Roof Systems.” *Renewable and Sustainable Energy Reviews*,77, 451–460.
52. Thaxton, C. S., Calantoni, J., & Mclaughlin, R. A. (2004). “Hydrodynamic Assessment of Various Types of Baffles in a Sediment Retention Pond. *Transactions of the American Society of Agricultural Engineers*, 47(3), 741-749.
53. Travis, Q. B., Asce, M., Mays, L. W., & Asce, F. (2008). “Optimizing Retention Basin Networks.” *Journal Of Water Resources Planning and Management*, 134(5), 432–439.
54. United States Environmental Protection Agency (2000). “Stormwater Phase II Final Rule: Construction Site Runoff Control Minimum Control Measure.” Washington, DC.
55. United States Environmental Protection Agency (2008). “Cool Roofs.” In: Reducing Urban Heat Islands: Compendium of Strategies. Draft. https://www.epa.gov/heat-islands/heat-island-compendium.
56. Vaughan, B. T., & Jarrett, A. R. (2001). “Experimental Evaluation of Alternative Configurations for Floating Riser Sedimentation Basin Dewatering Devices.” *2001 ASAE Annual Meeting*. Sacramento, CA.
57. Ward, A. D., Haan, C. T., & Barfield, B. J. (1979). “Prediction of Sediment Basin Performance.” *Transactions of the American Society of Agricultural Engineers*, 22(1), 126–136.
58. Wray, C., & Akbari, H. (2008). The Effects of Roof Reflectance on Air Temperatures Surrounding a Rooftop Condensing Unit.” *Energy and Buildings*, 40(1), 11–28.
59. Xu, T., Sathaye, J., Akbari, H., Garg, V., & Tetali, S. (2012). “Quantifying the direct benefits of cool roofs in an urban setting: Reduced cooling energy use and lowered greenhouse gas emissions.” *Building and Environment*, 48(1), 1–6.

60. Yang, J., & Bou-Zeid, E. (2019). “Scale dependence of the benefits and efficiency of green and cool roofs.” *Landscape and Urban Planning*, 185, 127–140.

61. Zech, W. C., Logan, C. P., & Fang, X. (2014). “State of the Practice: Evaluation of Sediment Basin Design, Construction, Maintenance, and Inspection Procedures.” *Practice Periodical on Structural Design and Construction*, 19(2).